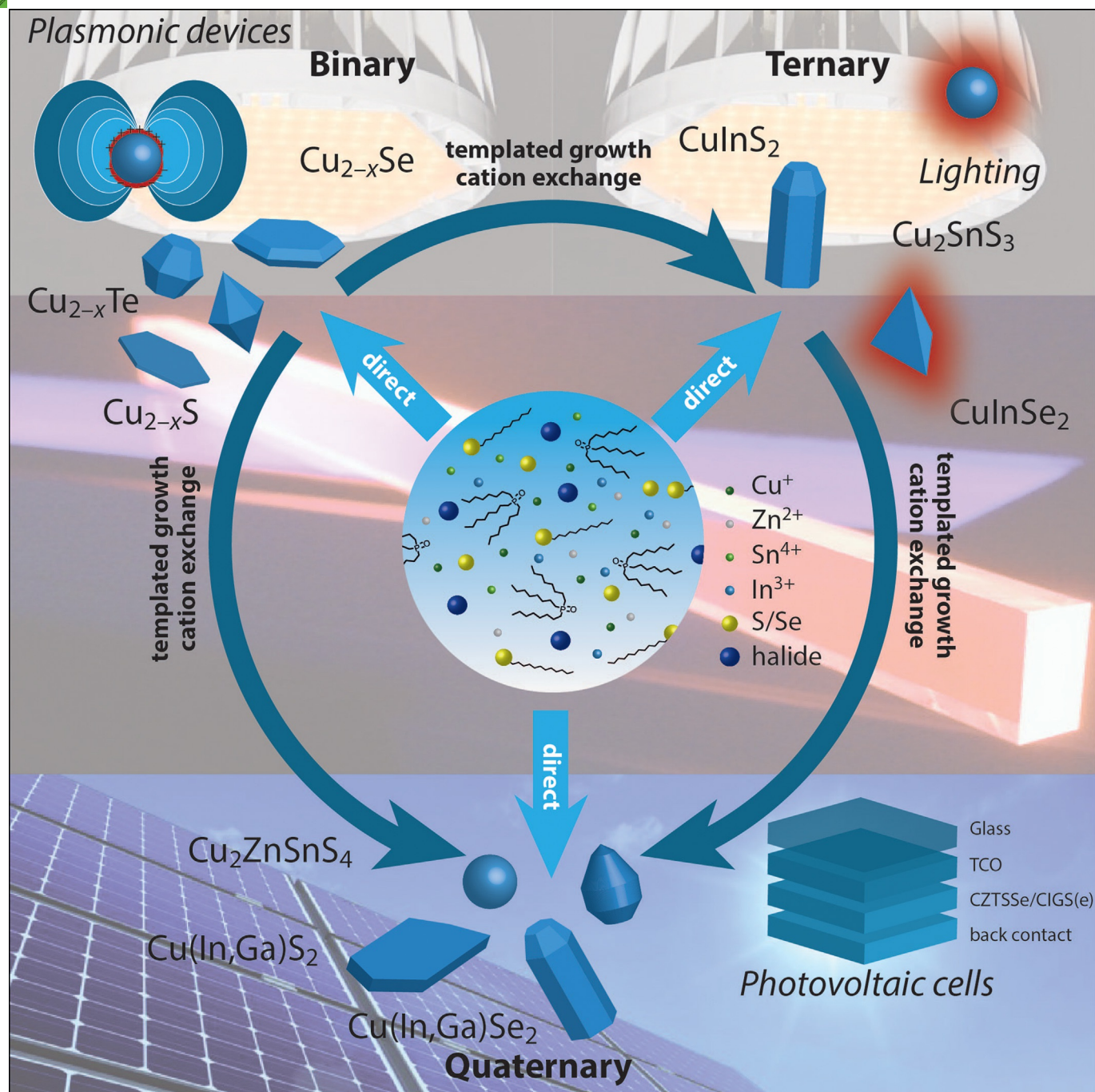VIP *Very Important Paper*

Prospects of Colloidal Copper Chalcogenide Nanocrystals

Ward van der Stam, Anne C. Berends, and Celso de Mello Donega*[a]

Over the past few years, colloidal copper chalcogenide nanocrystals (NCs) have emerged as promising alternatives to conventional Cd and Pb chalcogenide NCs. Owing to their wide size, shape, and composition tunability, Cu chalcogenide NCs hold great promise for several applications, such as photovoltaics, lighting and displays, and biomedical imaging. They also offer characteristics that are unparalleled by Cd and Pb chalcogenide NCs, such as plasmonic properties. Moreover, colloidal Cu chalcogenide NCs have low toxicity, potentially lower costs, and excellent colloidal stability. This makes them attractive materials for the large-scale deployment of inexpensive, sustainable, and environmentally benign solution-processed devices. Nevertheless, the synthesis of colloidal Cu chalcogenide NCs, especially that of ternary and quaternary compositions, has yet to reach the same level of mastery as that available for the prototypical Cd chalcogenide based NCs. This review provides a concise overview of this rapidly advancing field, sketching the state of the art and highlighting the key challenges. We discuss recent developments in the synthesis of size-, shape-, and composition-controlled NCs of Cu chalcogenides, with emphasis in strategies to circumvent the limitations arising from the need to precisely balance the reactivities of multiple precursors in synthesizing ternary and quaternary compositions. In this respect, we show that topotactic cation-exchange reactions are a promising alternative route to complex multinary Cu chalcogenide NCs and hetero-NCs, which are not attainable by conventional routes. The properties and potential applications of Cu chalcogenide NCs and hetero-NCs are also addressed.

1. Introduction

Colloidal semiconductor nanocrystals (NCs) have unique size- and shape-dependent properties that emerge once the NC dimensions reach the quantum confinement regime.[1] If the dimensions and shape of the NCs are such that the exciton is confined in all directions, a colloidal quantum dot (QD) is obtained. Similarly, NCs in which the exciton is confined only in the diameter direction are referred to as quantum wires (QWRs), whereas 2D confinement (i.e. thickness direction only) results in a quantum well (QWL). Quantum rods (QRs) are NCs in transition from the 0D to 1D confinement regime. Over the last decades, a wide variety of colloidal QDs, QRs, QWRs, and, more recently, QWLs have been developed and have been shown to have remarkable properties.[1, 2]

The possibilities for property engineering can be extended even further by combining two (or more) different semiconductors in the same NC through nanoscale heterojunctions (i.e. a hetero-NC, HNC). The carrier localization regime can then be tailored from type I (electron and hole in the same material) to type II (spatially separated charge carriers) through an intermediate regime (type I$^{1/2}$, one carrier delocalized over the whole volume of the HNC and the other localized in one of the segments) by controlling the composition, size, and shape of each segment of the HNC.[1] This offers a remarkable degree of control over the properties of nanoscale excitons in HNCs. Moreover, colloidal NCs and HNCs can be seen as hybrid inorganic–organic nanomaterials, as they are coated with a layer of organic ligand molecules, which make them highly amenable to surface manipulation and solution processing.[1] These characteristics have turned colloidal NCs and HNCs into promising materials for a wide variety of applications (e.g. optoelectronics, photonics, spintronics, catalysis, solar energy conversion, thermoelectrics, information processing and storage, sensors, and biomedical applications).[1]

The combination of exciting fundamental challenges and prospects for technological breakthroughs has motivated research groups worldwide to extensively investigate the synthesis and optoelectronic properties of a wide variety of semiconductor NCs and HNCs. Most of the work has been focused on Cd chalcogenides (particularly on the prototypical CdSe) and, more recently, on Pb chalcogenides. As a result, the synthesis of colloidal NCs and HNCs based on Cd and Pb chalcogenides has developed into a very mature field, which has led to materials with exceptional properties that have already demonstrated great potential for many applications (e.g. low-threshold lasing, light-emitting diodes, labels for biomedical imaging, photodetectors, and solar cells).[3–8] However, the large-scale deployment of these conventional QDs, QRs, QWRs, and QWLs is severely hindered by restrictions imposed on devices containing toxic elements such as Cd and Pb. This has stimulated growing interest in alternative materials that possess comparable properties and that are based on less-toxic elements.

Copper chalcogenides are a very attractive option, as they have low toxicity, environmental compatibility, potentially lower costs, and a very wide range of compositions and crystal structures. This latter point makes them an extremely versatile class of materials, capable not only of offering similar properties to those already demonstrated by Cd and Pb chalcogenide NCs and HNCs but also characteristics that are unparalleled by conventional NCs and HNCs (e.g. plasmonic properties). However, the synthesis of colloidal copper chalcogenide NCs and HNCs, especially that of ternary and quaternary compositions, is still largely underdeveloped and has yet to reach the same level of mastery as that available for the prototypical Cd chalcogenide based NCs and HNCs. As a result, comprehensive understanding of the optoelectronic properties of copper chalcogenides has yet to emerge. Nevertheless, the field is progressing fast, and there have been many recent advances.

[a] W. van der Stam, A. C. Berends, Dr. C. de Mello Donega
Debye Institute for Nanomaterials Science, Utrecht University
P.O. Box 80000, 3508 TA Utrecht (The Netherlands)
E-mail: c.demello-donega@uu.nl

ORCID(s) from the author(s) for this article is/are available on the WWW under http://dx.doi.org/10.1002/cphc.201500976.

An invited contribution to a Special Issue on Beyond Conventional Quantum Dots

In this review, we intend to provide an overview of the field, in which the state of the art is briefly outlined and critically discussed to highlight the essential issues and challenges that have yet to be addressed to promote further progress. This review is not intended as an exhaustive treatise, but rather as a concise account of some of the key aspects. For further details, the reader is referred to a number of recent reviews focusing on different topics within the field of copper chalcogenide nanocrystals.[9–12] The review is divided into three sections: binary copper chalcogenides, ternary copper chalcogenides, and quaternary copper chalcogenides.

2. Binary Copper Chalcogenides

Colloidal binary copper chalcogenide ($Cu_{2-x}A$; A = S, Se, and Te) NCs have attracted increasing attention over the last decade, because their properties make them interesting materials for implementation into several applications, such as solution-processable photovoltaic and nanoplasmonic devices, photocatalysis, photothermal therapy, and biomedical sens-

Ward van der Stam earned his MSc degree in Chemistry from Utrecht University in 2012. Currently, he is working as a PhD student in the Condensed Matter and Interfaces group at Utrecht University in the Netherlands. His research mainly focuses on tailoring the size, shape, and composition of Cu chalcogenide nanocrystals by direct synthesis methods, as well as cation-exchange reactions.

Anne Berends received her MSc degree in Chemistry from Utrecht University in 2014. She is currently working as a PhD candidate within the Debye Institute for Nanomaterials Science of the same university, investigating the synthesis and optical properties of $CuInS_2$ colloidal nanocrystals.

Dr. Celso de Mello Donega is an Associate Professor in the Chemistry Department of the Faculty of Sciences at Utrecht University in the Netherlands. He obtained his PhD degree in Chemistry from Utrecht University in 1994. His research is focused on the chemistry and optoelectronic properties of nanomaterials, with particular emphasis on colloidal nanocrystals and hetero-nanocrystals of semiconductors.

ing.[9, 10, 13–17] Some of these applications will be addressed in more detail in Section 2.4. To realize these applications, the size, shape, and polydispersity of the NC ensemble must be strictly controlled, as these characteristics are crucially important not only for the optoelectronic properties of the NCs themselves but also for the quality of the NC thin films obtained by solution-based deposition techniques.[18] This has motivated an extensive worldwide research effort into colloidal synthesis methods for $Cu_{2-x}A$ NCs, which has resulted in a remarkable degree of control over the size and shape of colloidal $Cu_{2-x}A$ NCs.[19–24]

2.1. Crystal Structure of Binary Copper Chalcogenides

The most investigated copper chalcogenide is $Cu_{2-x}S$, which can easily accommodate Cu vacancies. As a result, the binary Cu–S system has a very rich phase diagram,[25] with a variety of equilibrium crystal structures: monoclinic low-chalcocite α-Cu_2S, hexagonal high-chalcocite β-Cu_2S, monoclinic djurleite $Cu_{1.96}S$, hexagonal digenite $Cu_{1.8}S$, monoclinic roxbyite $Cu_{1.78}S$, orthorhombic anilite $Cu_{1.75}S$, and hexagonal covellite CuS. These crystal structures are characterized by either hexagonal or cubic close packing of the S atoms, with Cu atoms positioned at the interstices. Rearrangement of the S atoms from cubic to hexagonal (and vice versa) is extremely slow, and therefore, a number of metastable phases is also possible.[25] The crystal structure of $Cu_{2-x}Se$ is also determined by the number of Cu vacancies. The crystal structures range from klockmannite hexagonal $CuSe$,[26] umangite tetragonal Cu_3Se_2,[26] and berzelianite cubic $Cu_{2-x}Se$[26] to bellidoite cubic Cu_2Se.[26–29] Copper telluride can exist as orthorhombic CuTe; hexagonal Cu_2Te, Cu_3Te_4, and Cu_7Te_5; and as nonstoichiometric $Cu_{2-x}Te$ phases.[30–32]

2.2. Colloidal Synthesis of $Cu_{2-x}A$ Nanocrystals

The compositional and structural diversity of binary copper chalcogenides creates a very rich parameter space that can be exploited to tailor the size and shape of colloidal $Cu_{2-x}A$ NCs over a very wide range, opening up routes towards a plethora of morphologies not attainable for other binary semiconductor NCs. For example, nanodisks, nanoplatelets, (ultrathin) nanosheets, and other polyhedral shapes have been successfully synthesized with astonishingly narrow size and shape distributions (Figure 1).[19–24] As will be discussed below, by strictly controlling the reaction conditions (e.g. nature of precursors and ligands, concentrations, reaction temperatures), desired compositions and crystal structures can be obtained. This determines the chemical and crystallographic nature of the facets of the nascent NC, which in turn dictates the fate of NC growth, as the growth kinetics of the individual facets are governed both by their intrinsic free energies and by their affinity for the ligands present in the growth solution.[1]

$Cu_{2-x}A$ NCs with narrow size and shape distributions have been prepared by both hot-injection and heating-up synthesis protocols.[19–24, 33–37] The heating-up process typically results in larger NCs;[20, 22, 34] this suggests that the heating rates are not
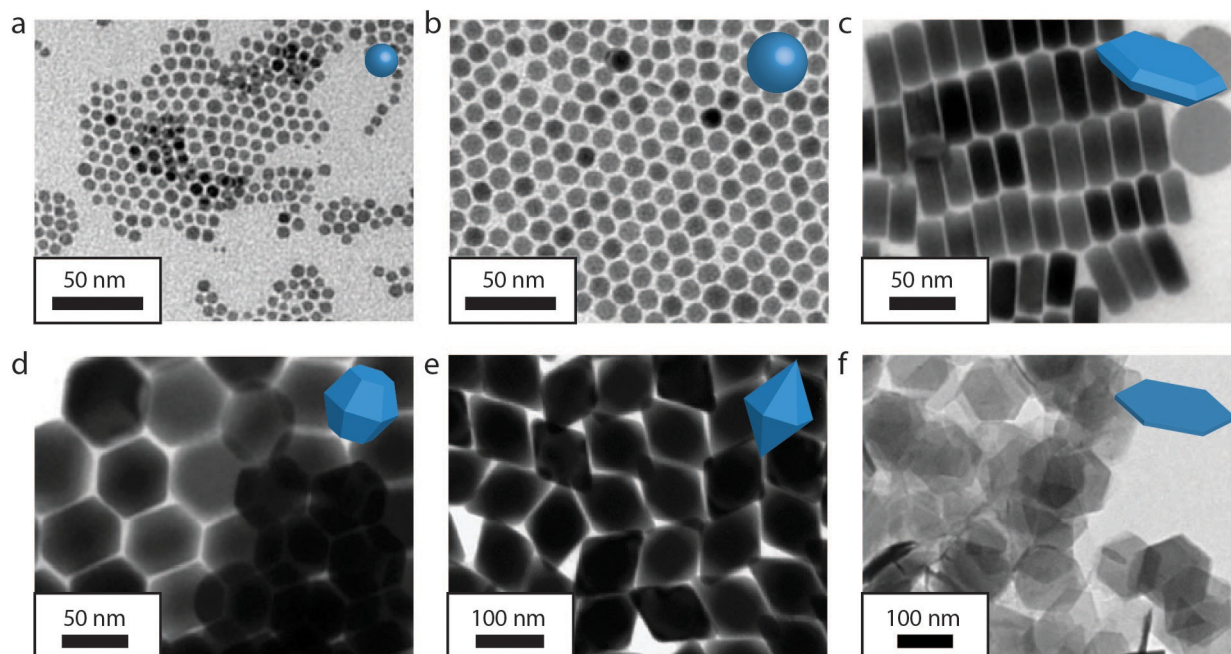
Figure 1. Size and shape control of colloidal $Cu_{2-x}S$ nanocrystals (NCs). By choosing the right synthetic parameters, the size and shape of colloidal $Cu_{2-x}S$ NCs is controlled from a,b) spherical NCs with different diameters (3–10 nm) to anisotropic NCs such as c) hexagonal nanoplatelets (thickness 20 nm, lateral dimensions 50 nm), d) bifrustums (50 nm), e) bipyramids (50 nm width by 100 nm length), and f) ultrathin nanosheets (thickness 2 nm, lateral dimensions 110 nm). The panels were adapted with permission from Refs. [23] (panels a,b, Copyright 2010 IOP Publishing), [22] (panels c–e, Copyright 2011 The Royal Society of Chemistry), and [24] (panel f, Copyright 2015 American Chemical Society).

sufficiently fast to induce a sudden burst of monomer formation from the precursors, which thereby results in relatively slow nucleation rates. This implies that the precursor to monomer formation is the rate-limiting step in the synthesis of colloidal $Cu_{2-x}A$ NCs, in line with the general mechanism proposed for the formation of colloidal NCs of metal chalcogenides.[1] This is also illustrated by the use of Cu^{II} salts for the synthesis of $Cu_{2-x}A$ NCs,[23,33] which introduces one additional kinetic step in the induction period, as the Cu^{2+} ions must first be reduced to Cu^+ before [CuA] monomers can form. This also stalls nucleation, which leads to fewer nuclei and, hence, larger NCs. It is, thus, clear that the precursor reactivities are one of the key factors in the synthesis of $Cu_{2-x}A$ NCs with narrow size and shape distributions.

The exact formation mechanism of colloidal $Cu_{2-x}A$ NCs is, however, still under debate. Cabot and co-workers have proposed an oriented attachment pathway through which hexagonal nanodisks form hexagonal $Cu_{2-x}S$ bifrustums and eventually hexagonal bipyramids.[22] Other groups have presented evidence that Cu thiolate lamellar complexes act as both Cu precursors and shape-templating agents.[15,24,38,39] Recent work has demonstrated that the crystallographic phase and composition of $Cu_{2-x}S$ NCs (see Section 2.1) can be controlled by proper choice of reaction parameters (namely, temperature, molar ratio of Cu/S, and volume ratio between the noncoordinating solvent 1-octadecene and the ligand oleylamine).[40] The addition of ligands has also been used as a shape-control strategy.[20,21] Ligands usually have a preferred crystallographic facet to which they bind.[1,41] Therefore, by choosing the right surfactants, chemists have been able to produce anisotropically

shaped NCs such as 1D CdSe and CdS nanorods (phosphonic acid as ligands)[41] or 2D CdSe nanosheets (oleic acid as ligands).[2] Typically, organic surfactant molecules are commonly used, whereas inorganic ligands have only recently emerged to stabilize nanomaterials in polar solvents such as water and ethanol.[42,43] These advances for Cd-based nanomaterials may lead to synthetic strategies resulting in designed Cu chalcogenide architectures with tailored surface functionalities, which may prove beneficial for the implementation of these NCs into devices and bioapplications.

Nevertheless, the synthesis protocols for colloidal $Cu_{2-x}A$ NCs are also subject to limitations, especially in the case of selenides and tellurides, for which very few anion precursors are available. Several chalcogenide precursors have been reported, but the most extensive library is that of the sulfide precursors. The most commonly used sulfide precursors are tri-n-octylphosphine sulfide (TOP-S), 1-dodecanethiol (DDT), thiourea, bis(dimethylsilyl)sulfide, and elemental sulfur dissolved in 1-octadecene (S-ODE).[11,12] The use of the selenide and telluride analogues of these precursors is hindered by stability issues. In fact, only TOP-Se and TOP-Te are suitable precursors in terms of stability and reactivity, but the presence of TOP (a soft Lewis acid) is undesirable, as it strongly binds to the Cu^+ ions (a soft Lewis base),[44] which thereby slows the nucleation rates and enhances ripening. In some cases, Se-ODE is used as a precursor, but the poor solubility of Se in ODE leads to relatively large and polydisperse NCs.[27,28,45,46] Selenourea has emerged as an alternative, but the resulting NCs are limited in terms of size and shape, as only large NCs are obtained.[47] Moreover, Te is almost completely insoluble in ODE. An alternative is to mix

all reactants, including the elemental chalcogen as a powder, and to heat the mixture up to the reaction temperature.[48] However, this method offers limited size and shape control. Therefore, the search for a suitable Se/Te precursor that allows for size- and shape-controlled growth of $Cu_{2-x}A$ NCs continues.

Limitations in the synthesis of $Cu_{2-x}A$ NCs can also be circumvented by using cation-exchange reactions. For example, ultrathin $Cu_{2-x}Se$ nanoplatelets,[49] $Cu_{2-x}S$ nanowires,[50] $Cu_{2-x}Te$ QDs, nanorods, and tetrapods[51] and several Cu_2Se/Cu_2S core–shell HNC architectures,[52–54] which cannot be prepared by direct synthesis, have been obtained from template Cd-based NCs by topotactic Cd^{2+} for Cu^+ cation exchange.

2.3. Superlattices of $Cu_{2-x}A$ Nanocrystals

The narrow size distribution of the colloidal $Cu_{2-x}A$ NCs produced by the methods discussed above allow them to readily self-assemble into ordered 3D superstructures (Figure 2). This may prove beneficial for the successful implementation of $Cu_{2-x}A$ NCs into photovoltaics and other optoelectronic devices. The tunability of the size and shape of $Cu_{2-x}A$ NCs offers another possibility to tune the geometry and, therefore, the properties of the self-assembled superlattices. Given that $Cu_{2-x}A$ NCs can grow anisotropically or have polyhedral shapes, the packing geometry can be altered, ranging from face-centered cubic to hexagonal close packing (Fig-ure 2 a,b),[55] or to corncob-like superstructures (Figure 2 c),[56] long-range stacking of nanoplatelets (Figure 2 e)[20] and nano-sheets (Figure 2 f).[24]

2.4. Properties and Potential Applications of $Cu_{2-x}A$ Nanocrystals

2.4.1. Photovoltaic Applications

Copper chalcogenides are p-type semiconductors, regardless of the chalcogenide. $Cu_{2-x}S$ is a direct semiconductor with a bandgap that depends on its stoichiometry (1.1–1.4 eV for djurleite, $x=0$–0.04; 1.5 eV for digenite, $x=0.2$; 2.0 eV for covellite, $x=1$).[33,55,57] $Cu_{2-x}Te$ also has a direct bandgap that can be tuned between 1.1 and 1.5 eV, depending on its stoichiometry.[30–32] In contrast to $Cu_{2-x}S$ and $Cu_{2-x}Te$, $Cu_{2-x}Se$ has been reported to have both direct and indirect band gaps (2.1–2.3 and 1.2–1.4 eV, respectively).[16,27,28]

The combination of a suitable band gap, high absorption coefficient (10^4 cm^{-1}), low cost, and low toxicity has made $Cu_{2-x}S$ a prime candidate for the large-scale and sustainable deployment of photovoltaics (PVs).[21,58,59] In fact, CdS/Cu_2S heterojunction solar cells were among the earliest thin-film solar cells to be investigated, but their further development was hindered by the low stability of the p/n junction, which deteriorated in air due formation of Cu vacancies and Cd–Cu interdif-
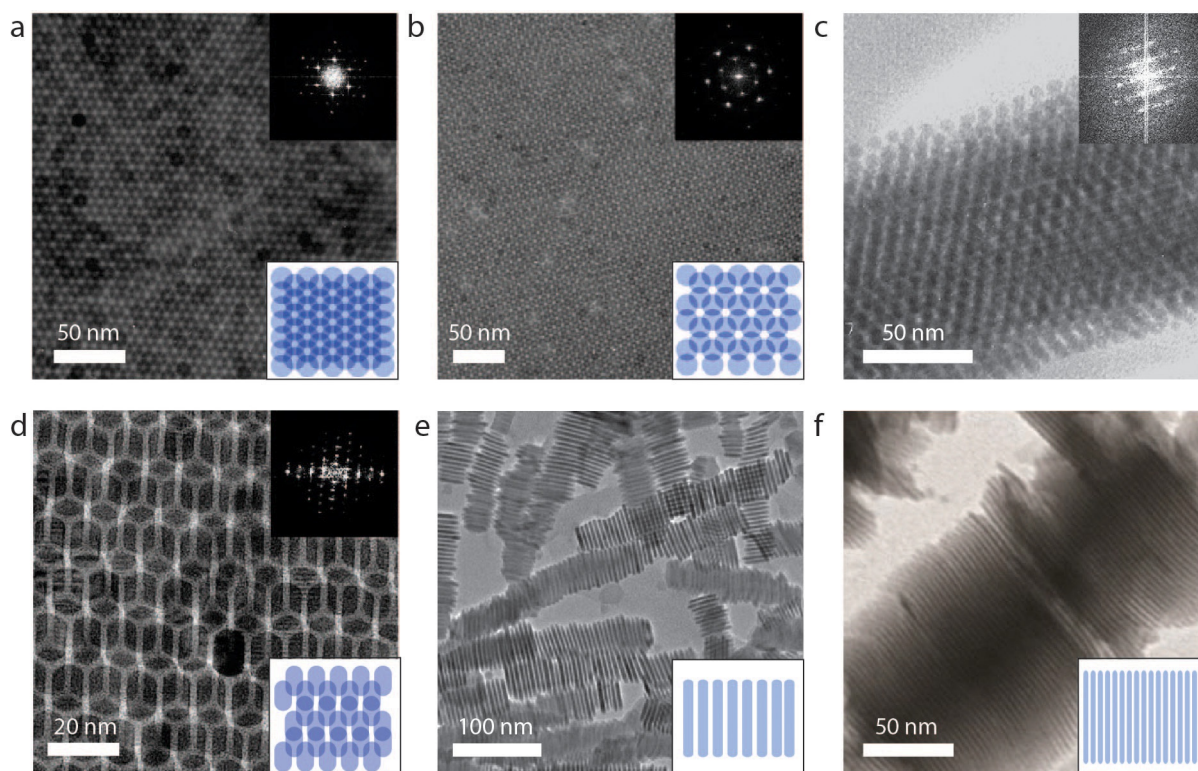

Figure 2. Self-assembled 3D superstructures of $Cu_{2-x}S$ nanocrystals. Spherical $Cu_{2-x}S$ NCs readily self-assemble into a variety of ordered 3D superstructures, such as a,b) hcp and c) corncob structures. d) Self-assembly of anisotropic NCs results in distortion of the hcp packing to a rhombohedral geometry. e) $Cu_{2-x}S$ nanoplatelets and f) ultrathin nanosheets form stacks. The panels were adapted with permission from Refs. [55] (panels a,b,d; Copyright 2008 American Chemical Society), [56] (panel c, Copyright 2009 Elsevier), [20] (panel e; Copyright 2010 American Chemical Society), and [24] (panel f, Copyright 2015 American Chemical Society).

fusion.[9,22,60] The possibility to make colloidal dispersions of monodisperse $Cu_{2−x}S$ NCs has renewed interest in $Cu_{2−x}S$ for PVs,[9,61–67] as it allows the fabrication of solar cells by solution-deposition techniques, such as ink-jet printing by using nanocrystal inks. Nevertheless, ternary and quaternary copper chalcogenides have superior environmental stability and efficiency and are, therefore, preferred in the fabrication of PV devices (see Sections 3.3.2 and 4.3.1). However, $Cu_{2−x}S$ NCs show promise as low-costing counter electrodes for dye- or QD-sensitized solar cells.[40]

2.4.2. Optical Properties of Cu2−xA Nanocrystals and Plasmonics

As mentioned above (Section 2.4.1), the band gap of $Cu_{2−x}A$ increases with the copper deficiency x. This has been explained by an increase in the concentration of free carriers (holes) in the material as a result of the introduction of copper vacancies.[9] The excess holes will occupy the top of the valence band, which thereby increases the effective band gap (i.e. the Moss–Burstein effect).[68] This effect also leads to a low-energy absorption tail in the spectra of $Cu_{2−x}A$ NCs, which makes precise determination of the NC band gap difficult. This also typically precludes clear observation of the lowest energy exciton transitions in NCs that are sufficiently small to experience quantum confinement effects (the estimated exciton Bohr radius in Cu_2S is ≈ 5 nm[13,57]). Interestingly, the hole concentration in $Cu_{2−x}A$ NCs is sufficiently high to give rise to localized surface plasmon resonances (LSPRs).[13] For example, metallic-like covellite CuS NCs display a broad absorption band in the near-IR region, which is associated with a LSPR of free holes introduced in the material by the copper vacancies ($x=1$ in CuS, but the Cu atoms are still in the $+1$ oxidation state[33]). The LSPR can be tuned by introducing additional Cu^+ ions

(Figure 3), which decreases the concentration of free holes and thereby weakens the LSPR and simultaneously shifts it to lower energies.[33] Once the fully stoichiometric Cu_2S composition is reached, the LSPR band is completely damped, and the radiative recombination of the exciton becomes observable.[51] The same holds for $Cu_{2−x}Se$ NCs, in which the LSPR band can be damped by the addition of Cu^+ ions or enhanced by oxidation of the NCs with O_2 or Ce^{IV}.[69] The near-IR LSPR of $Cu_{2−x}A$ NCs can also be damped by incorporating other metal ions (such as In^{3+}).[70] This shows that $Cu_{2−x}A$ NCs possess the unique property of holding excitons and highly tunable LSPRs on demand (Figure 3).[28,31,33,34,51,57,69] The LSPR band of $Cu_{2−x}A$ NCs has been shown to depend not only on the composition of the NCs but also on their size[13] and shape.[71,72] The combination of these characteristics makes $Cu_{2−x}A$ NCs promising materials for photovoltaics,[59] photocatalysis,[73] and nanoplasmonics.[13,51,57]

2.4.3. Cu2−xA Nanocrystals as Templates for Topotactic Nanoscale Cation-Exchange Reactions

Nanoscale cation exchange (CE) offers a versatile alternative for direct-synthesis protocols, as it allows for postsynthetic control over the NC composition, while preserving the size and shape of the parent NCs.[74–83] Colloidal $Cu_{2−x}A$ NCs, prepared by direct-synthesis protocols, are often used as parent (template) NCs in CE reactions to yield other metal chalcogenide NCs.[74–77,82] In this way, the size and shape control already achieved for $Cu_{2−x}A$ NCs can be translated to other metal chalcogenides.

The Cu^+ ions in copper chalcogenides have been shown to be easily exchangeable by other cations,[74–77,82] mainly because of their small size and charge, which results in fast diffusion through the anionic sublattice. These characteristics, in combi-
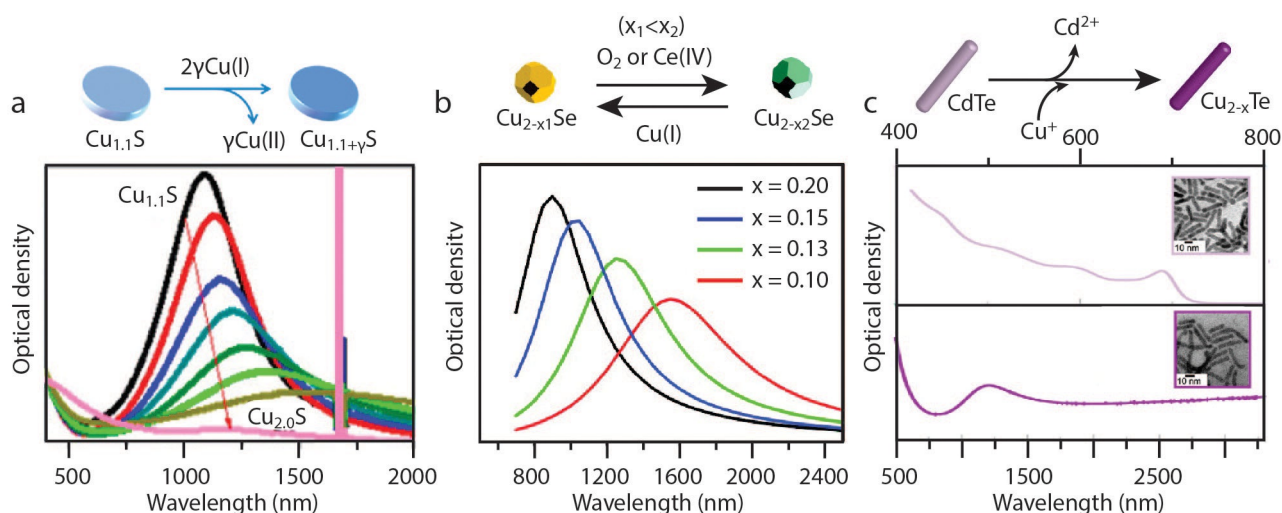

Figure 3. Localized surface plasmon resonance (LSPR) in Cu chalcogenide NCs. Cu chalcogenide NCs have tunable LSPR, which can be enhanced by oxidizing the NCs or damped by reducing the NCs. a) The LSPR in $Cu_{2−x}S$ NCs is tuned between 1000 and 1500 nm, whereas b) $Cu_{2−x}Se$ NCs can hold LSPR between 800 and 1600 nm. c) LSPR around 1000 nm has been observed in $Cu_{2−x}Te$ nanorods, obtained by Cu^+ for Cd^{2+} cation exchange. The panels were adapted with permission from Refs. [33] (panel a, Copyright 2013 American Chemical Society), [69] (panel b, Copyright 2011 American Chemical Society), and [51] (panel c, Copyright 2013 American Chemical Society).

nation with the availability of Cu-extracting ligands, make it possible to effectively extract Cu^+ ions from the NCs and to replace them with other cations, without disrupting the anionic sublattice. Alkylphosphines, such as tri-n-octylphosphine (TOP), are commonly used to extract Cu^+ from NCs,[74–77,82] due to the strong affinity of the soft Lewis acid Cu^+ (absolute hardness $\eta = 6.28$ eV)[44] and the soft base TOP ($\eta = 6$ eV).[44] In this way, NCs can be obtained with unprecedented sizes, shapes, and crystal structures. For example, luminescent CdTe nanodisks (Figure 4a)[30] and InP nanoplatelets[80] have been obtained from template Cu_2Te and $Cu_{3−x}P$ NCs by topotactic M^{n+} (Cd^{2+} and In^{3+}, respectively) for Cu^+ cation exchange. Moreover, ZnS/Cu_2S hetero-nanocrystals have been prepared by partial Zn^{2+} for Cu^+ CE in $Cu_{1.8}S$ parent NCs, in which a thin slab of $Cu_{2−x}S$ remains between two cation-exchanged ZnS portions (Figure 4b).[81] Furthermore, we have recently shown that self-limited partial In^{3+} for Cu^+ CE reactions in $Cu_{2−x}S$ QDs can be used to prepare luminescent wurtzite $CuInS_2$ QDs[82] and near-IR-emitting $CuInSe_2/CuInS_2$ heteronanocrystals.[78]

Copper chalcogenide NCs are also often used as intermediates in sequential CE reactions, which makes it possible to synthesize NCs that would otherwise be inaccessible. In this way, PbS nanorods have been prepared from template CdS NRs by sequential (Cu^+ for Cd^{2+} followed by Pb^{2+} for Cu^+) CE reactions (Figure 4c).[76] Furthermore, wurtzite ZnSe/ZnS core–shell NRs[52] and ultrathin nanoplatelets[53] have been obtained by

sequential CE (Cu^+ for Cd^{2+} followed by Zn^{2+} for Cu^+) in template CdSe/CdS core–shell NRs (Figure 4d) and nanoplatelets, respectively.

3. Ternary Copper Chalcogenides

Unlike binary copper chalcogenides, ternary I–III–VI materials display tunable photoluminescence (PL) and are, therefore, promising alternatives to Cd and Pb chalcogenide NCs in several applications, such as light-emitting diodes,[84–86] photovoltaics,[87,88] luminescent solar concentrators,[89,90] bioimaging,[91,92] and photocatalysis.[93] Some of these potential applications will be addressed in more detail in Section 3.3.

3.1. Crystal Structure of Ternary Copper Chalcogenides

Ternary copper chalcogenides, with the general formula $CuXA_2$ (X = In, Sn, Ga, Al; A = S, Se, Te), exist at room temperature in the chalcopyrite crystal structure, a direct derivative of the binary zinc blende structure (Figure 5).[94] Another stable phase is the CuA_5X_8 spinel crystal structure, which also has a face-centered cubic (fcc) close packing of the anions. These bulk crystal phases can undergo phase transformations at elevated temperatures or at the nanoscale. For example, $CuInS_2$ (CIS) exists in the metastable wurtzite structure (Figure 5) at 1045 °C
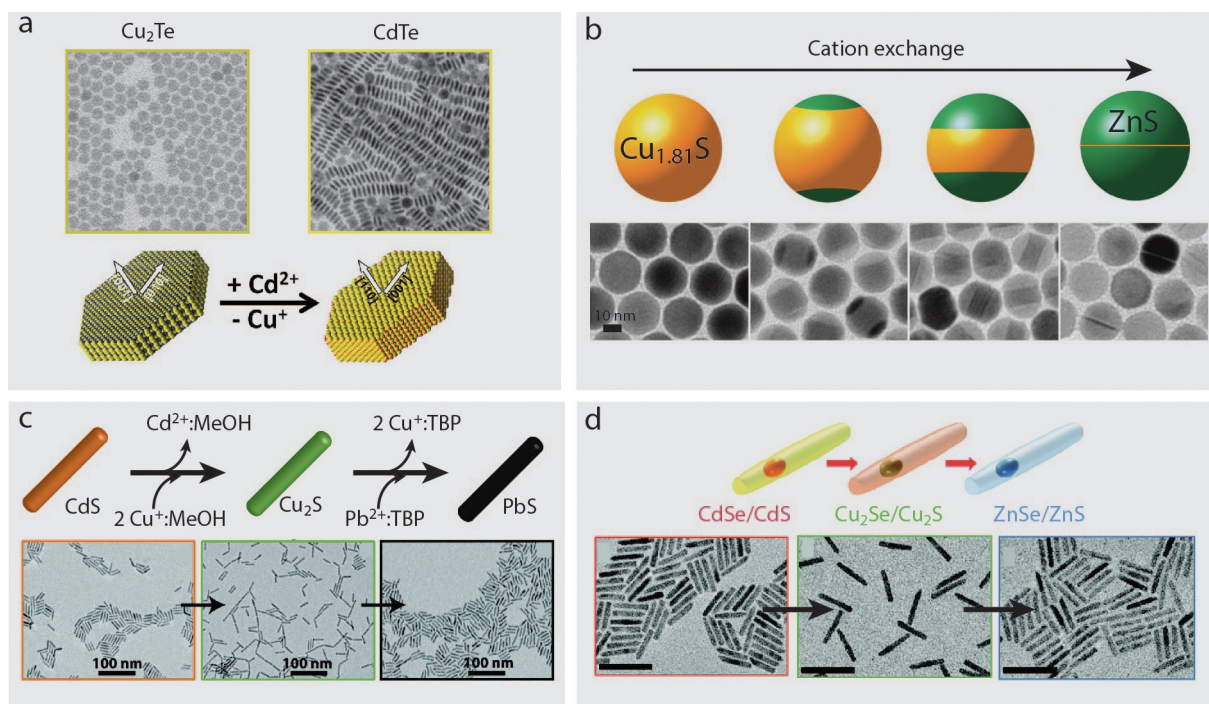

Figure 4. Cation-exchange reaction with binary Cu chalcogenide nanocrystals (NCs) as parent or intermediate NCs. Cation-exchange reactions in Cu chalcogenide NCs are commonplace and effectively result in NCs that are not attainable by direct synthesis. For example, a) CdTe nanodisks with visible PL have been obtained by using $Cu_{2−x}Te$ nanoplates as starting NCs. b) Partial Zn^{2+} for Cu^+ cation exchange in digenite $Cu_{1.8}S$ NCs results in hamburger-like Cu_2S-ZnS hetero-nanocrystals with a tunable Cu_2S portion depending on the reaction time. Sometimes, direct exchange is energetically unfavorable, and in those cases, Cu chalcogenide NCs serve as stable intermediate, as in the conversion of c) CdS nanorods into PbS nanorods via Cu_2S nanorods (TBP = tributylphosphine; scale bars: 100 nm) as well as d) CdSe/CdSe heteronanorods into ZnSe/ZnS heteronanorods via Cu_2Se/Cu_2S heteronanorods; scale bars: 50 nm. The panels were adapted with permission from Refs. [30] (panel a, Copyright 2013 American Chemical Society), [81] (panel b, Copyright 2014 American Chemical Society), [76] (panel c, Copyright 2009 American Chemical Society), and [52] (panel d, Copyright 2012 American Chemical Society).
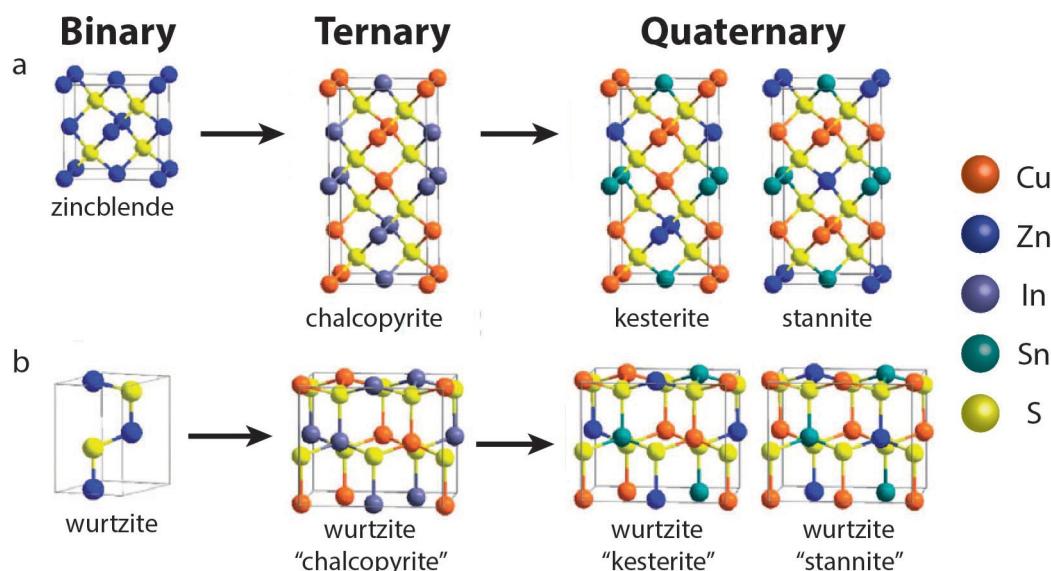
Figure 5. Crystal structures of ternary and quaternary Cu chalcogenide NCs. The crystal structures of ternary and quaternary Cu chalcogenides are derived from that of the binary analogues. a) If the binary NCs have a zinc-blende-like crystal structure, the resulting ternary NCs have the chalcopyrite crystal structure, whereas the quaternary NCs will have either stannite or kesterite structures. b) If cation-exchange reactions are deployed on wurtzite-like Cu chalcogenides, the resulting ternary and quaternary NCs also have a wurtzite structure. Adapted with permission from Ref. [94], Copyright 2013 The Royal Society of Chemistry.

in the bulk,[95] but wurtzite CIS NCs have been obtained at much lower temperatures[96] (see Section 3.2).

3.2. Colloidal Synthesis of Ternary Copper Chalcogenide Nanocrystals

The synthesis of colloidal NCs of ternary copper chalcogenides is still underdeveloped in comparison to that of II–VI and $Cu_{2-x}A$ NCs. This is primarily due to the fact that the control of the nucleation and growth rates of I–III–VI NCs is inherently more challenging, as the reactivities of two cation precursors and the anion precursor have to be finely tuned to prevent the formation of binary NCs and to achieve the targeted ternary composition. Therefore, the sizes and shapes of I–III–VI NCs are still limited. Furthermore, the exact growth mechanisms of ternary copper chalcogenide NCs are still under debate. Comprehensive reviews on the synthesis of ternary copper chalcogenide NCs have been recently published by Kolny-Olesiak and Weller[11] and Aldakov et al.[12] We will therefore restrict ourselves here to a brief discussion of the state of the art, with special emphasis on alternative ways that have been recently proposed to circumvent the limitations associated with the synthesis of $CuXA_2$ NCs.

The most widely investigated ternary copper chalcogenide composition is CIS, for which two stable crystal structures have been reported for NCs (Figure 6). Small, quasispherical CIS NCs with the chalcopyrite crystal structure (roquesite CIS, Figure 6a,b,e) and visible-to-near-IR-tunable PL have been synthesized by direct synthesis protocols.[97–102] The most common synthesis protocol for luminescent CIS NCs with diameters below 10 nm consists of heating a mixture of CuI (or CuAc), $In(Ac)_3$, and DDT.[11, 12, 97, 102] In this case, DDT plays the multiple roles of sulfur source, ligand, and solvent.

Large non-luminescent wurtzite CIS nanorods have been synthesized by using in situ nucleated $Cu_{2-x}S$ NCs as seed particles (Figure 6c,d,f).[96, 101] In this case, the hexagonal wurtzite crystal structure of the CIS nanorods is inherited from the $Cu_{2-x}S$ NC seeds (Figure 5), which also have a hexagonal crystal structure. At sufficiently high temperatures, CIS nucleates on the seed NCs, after which further growth of the CIS NCs happens at the heterointerface of the two materials; this consumes the Cu_2S NC seed as a sacrificial Cu^I and sulfur source. The size of the resulting CIS NCs is largely determined by the size of the Cu_2S seeds, which provides an additional way to control the size of the CIS NCs (Figure 7).

Another formation mechanism proposed for CIS NCs involves a $CuIn(SR)_x$ intermediate.[94, 102] The stability of this intermediate has been shown to have a crucial impact on the crystal structure of the resulting CIS NCs. For example, a stable intermediate (achieved by using low reaction temperatures or by adding coordinating ligands, such as oleylamine) results in wurtzite CIS NCs, whereas a less-stable intermediate leads to chalcopyrite CIS NCs. This highlights the influence that the surfactants and the reactivities of the precursors have on the resulting crystal structure and hence, the NC shape and faceting.[1]

Most synthesis protocols for ternary Cu sulfides use thiolate complexes as a sulfur source. Although thiols are an inexpensive alternative due to their multiple roles in the synthesis, they also impose additional energy barriers to the nucleation and growth of the NCs, as the C—S bonds of thiolate molecules must first undergo thermolysis. In this way, a limited amount of monomers are available, which results in limited control over the size, shape, and composition. Protocols to synthesize the Se analogue of CIS, $CuInSe_2$ (CISe), are similar to the ones used for CIS, except that Se is typically supplied in its elemen-
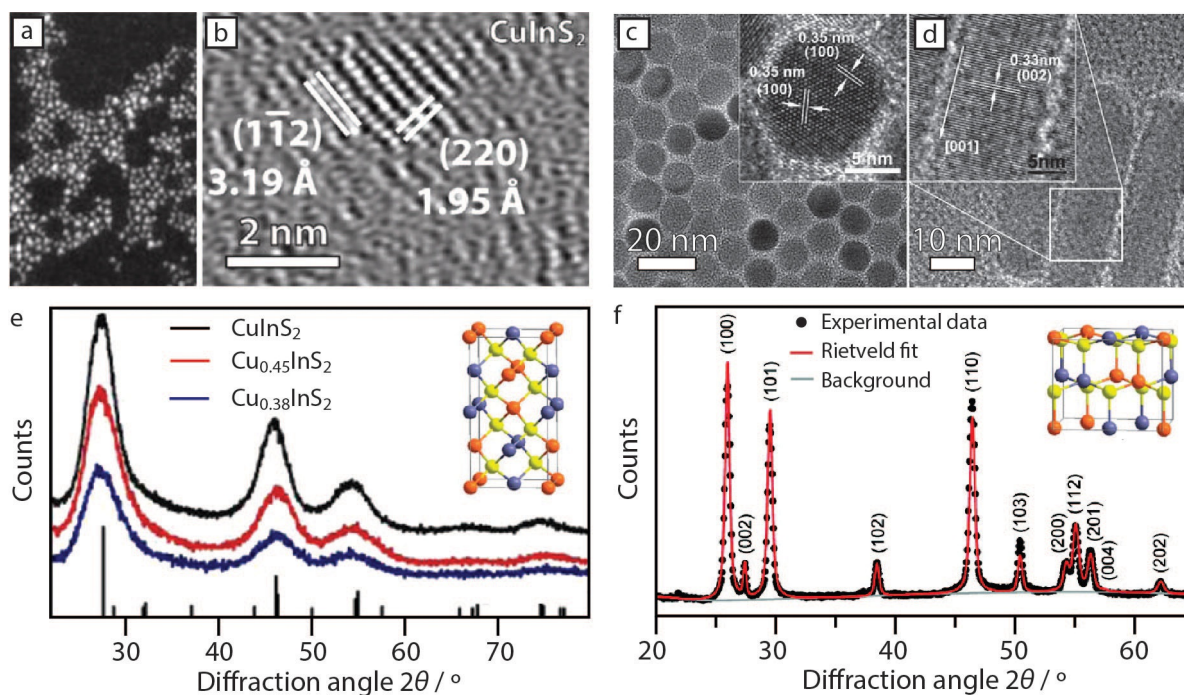
Figure 6. Chalcopyrite and wurtzite CuInS$_2$ NCs. Ternary CuInS$_2$ (CIS) NCs can attain two stable crystal structures, namely, chalcopyrite (zinc blende derivative) and wurtzite. a,b,e) Chalcopyrite CIS NCs typically form small, pyramidal NCs. c,d,f) Wurtzite CIS NCs are usually larger and often anisotropic. The panels were adapted with permission from Refs. [97] (panels a,b,e; Copyright 2012 American Chemical Society), [96] (panels c,d; Copyright 2011 The Royal Society of Chemistry), and [101] (panel f, Copyright 2010 American Chemical Society).
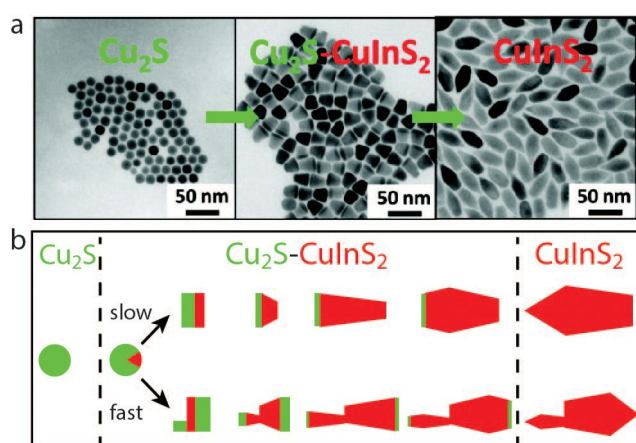

Figure 7. Growth mechanism of wurtzite CuInS$_2$ NCs. a) TEM images of the different stages of the reaction. b) The proposed growth mechanism states that first Cu$_2$S quasispherical NCs homogeneously nucleate. Second, a small domain of CIS nucleates heterogeneously onto the Cu$_2$S seeds. Depending on whether the heterogeneous nucleation is slow or fast, CIS grows on one or two sides of the seed. Cu$_2$S CIS hetero-NCs are isolated at intermediate reaction times, whereas at longer times homogeneous CIS NCs are obtained. Adapted with permission from Ref. [101], Copyright 2010 American Chemical Society.

tal form dissolved in coordinating solvents such as oleylamine,[103] as selenothiols are not readily available. The shapes reported for colloidal CISe NCs are trigonal pyramids,[47] bullets,[104] platelets,[103] dot-cuboctahedra,[105] and wires.[106,107]

Ternary copper tin chalcogenides (CTAs; A = S, Se, Te) have a large variety of stable phases, among which Cu$_2$SnA$_3$ is the most studied. Several reports show that the capping ligands present in the reaction mixture have a crucial impact on the crystal structure of the resulting CTS or CTSe NCs.[108,109] For example, cubic and wurtzite crystal structures have been reported by Ryan and co-workers upon using elemental selenium at elevated temperatures and diphenyl diselenide, respectively (Figure 8).[109] Diorgano dichalcogenides, such as diphenyl diselenide, are more reactive than elemental selenium (as Se^0 must first reduce to Se^{2-} before monomers can form), and therefore, the reaction can take place at lower temperatures. As a result, wurtzite NCs are formed at lower temperatures. The cubic crystal phase only forms at higher reaction temperatures, but with the additional precaution that the precursor reactivities are balanced so as to ensure that a ternary composition is formed.[109] Furthermore, synthesis protocols for Cu$_2$SnS$_3$ NCs involving Cu thiolate intermediates [CuSn(SR)$_x$] as a sulfur source have shown that, depending on the reaction temperature and solvent (i.e. octadecene or oleylamine), wurtzite or zinc blende NCs are formed.[94] Coordinating ligands can also play a pivotal role. For example, the removal of oleic acid from the reaction mixture has resulted in a change in crystal structure from wurtzite to kesterite (zinc blende derivative).[110] Up to date, the NC shapes accessible for CTS(e) NCs are ultrathin nanosheets with a very low Sn content,[111] tetrahedral NCs,[94,109] and tetrapods.[109]

More recently, Cu$_2$SnS$_3$ NCs have been produced by a hot-injection method, and the growth mechanism was studied in
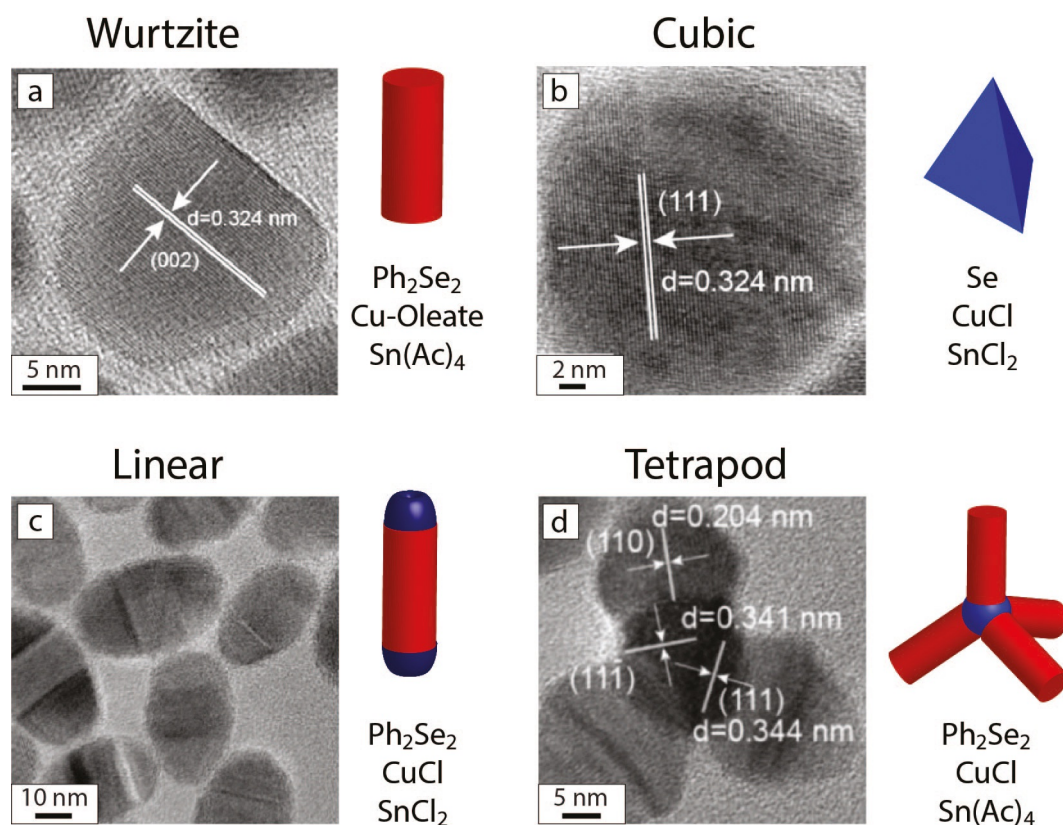
Figure 8. Size and shape control of ternary Cu_2SnSe_3 NCs and hetero-NCs. The size and shape of ternary Cu_2SnSe_3 NCs and hetero-NCs can be tuned by the respective precursor reactivities. For example, diphenyl diselenide as chalcogenide source results in a, c, d) hexagonal wurtzite crystal structures, whereas b) cubic NCs are obtained if elemental Se is used. The availability of a reactive Cu source plays an additional role, which results in c, d) hetero-NCs if halide ions are present. Adapted with permission from Ref. [109], Copyright 2014 American Chemical Society.

detail.[112] Two different ligands were used to control the reactivity of the different precursors in solution, which thereby controlled the shape of the product NCs. The first coordinating ligand, 1-dodecanethiol, is a soft Lewis base and therefore reacts with the soft Lewis acid Cu^+ to stabilize these ions in solution.[44] The second coordinating ligand, trioctylphosphine oxide, is a hard Lewis base that stabilizes the hard Lewis acid tin ions in solution.[44] Both of these ligands stabilize the surface copper and tin ions, respectively, upon incorporation into the NCs, which thereby directs the NC growth to hexagonal prismatic structures. Without these ligands and with only *tert*-dodecanethiol as sulfur source/ligand, elongated NCs form. To explain these observations, a multistep formation mechanism is proposed, in which djurleite copper sulfide NCs form first and are subsequently converted into orthorhombic Cu_2SnS_3 by Sn interdiffusion.[112]

3.2.1. Alternative Synthesis Routes to Ternary Copper Chalcogenide Nanocrystals

As illustrated above, the control over size, shape, and stoichiometry of ternary copper chalcogenide NCs through direct synthesis protocols is still limited. As discussed in Section 2.4.3, topotactic CE reactions have emerged as a promising alternative for direct synthesis protocols. In a typical CE reaction, (part

of) the cations of the parent NCs are exchanged by different cations, whereas the anionic sublattice remains unaffected.[74,113,114] The efficient extraction of the native cation with concomitant incorporation of the new cation, while preserving the size and shape of the NC, depends on multiple reaction parameters that must be well balanced, as an imbalance may lead to dissolution of the parent NCs or no exchange at all.[74,113,114] The most important parameters to control are the chemical potential of the cations in solution and in the NC. This chemical potential can be influenced, for example, by the choice of solvent, coordinating ligands, and cation precursor salts. The exact balance between these parameters is delicate and different for every system and, therefore, is often poorly understood. Nevertheless, CE is a powerful and exciting synthesis strategy that can lead to NCs with unprecedented compositions, shapes, and crystal structures that would otherwise not be attainable.[74–83] Below, we will discuss some recent examples of partial CE reactions from binary to ternary copper chalcogenide materials. This partial exchange requires either a very precise determination of concentrations, such that only part of the cations can be replaced, or a very good understanding of the mechanism involved, such that the CE reaction is self-limited.

For example, we have recently shown a self-limited partial CE reaction from $Cu_{2−x}S$ NCs to luminescent ternary CIS NCs.[82]

In this case, the Cu^+ ions (soft Lewis acids) are extracted by TOP (a soft Lewis base), whereas In^{3+} forms a $[In(MeOH)_x]^{3+}$ complex with solvent molecules that transports it to the NC surface (Figure 9a). We found that the balance between the Cu_{out} and In_{in} diffusion rates is delicate and can only be achieved under mild reaction conditions (room temperature), resulting in self-limited partial CE, which stops once the ternary composition is reached. To proceed until the fully exchanged composition, In_2S_3, is obtained, a large energy barrier must be overcome due to the anionic rearrangement required for this transformation. The template $Cu_{2-x}S$ NCs and the ternary product CIS NCs both have a hexagonal crystal structure with hexagonal close packing (hcp) of anions (chalcocite and wurtzite, respectively), whereas In_2S_3 has a fcc packing of anions (Figure 9b,c). Although possible, this transformation from hcp to fcc requires a lot of energy, which is not available at the low temperatures used in the reaction.[115]

We have extended this synthesis strategy to anisotropic and complex HNCs by adapting the cation-exchange protocol in such a way that the ingoing and outgoing diffusion rates are effectively coupled, which thereby prevents imbalances and makes it possible to obtain luminescent ternary $CuInSe_2/CuInS_2$ core–shell heteronanorods (Figure 9e).[78] This can be achieved by using a stoichiometric TOP–$InCl_3$ complex as both the In source and the Cu-extracting agent (Figure 9d). This method has also been applied to other ternary compositions to yield a variety of ternary (hetero)structures that are not attainable by direct routes, which thus paves the way toward a plethora of ternary NCs with tailor-made sizes, shapes, compositions, and heteroarchitectures.[78]

Similar observations have been reported for other ternary Cu chalcogenide NCs prepared by partial CE reactions. For example, full conversion of $Cu_{2-x}Se$ NCs into SnSe NCs has been observed for CE with Sn^{2+} cations, whereas CE with Sn^{4+} cations results in self-limited partial CE to $Cu_{2-x-4y}Sn_ySe$ NCs.[116] This is explained by the easy diffusion of the Sn^{4+} ions through the NC lattice by hopping into copper vacancies, as Sn^{4+} and Cu^+ have similar radii.[116] This results in a gradual and isotropic replacement of the cations throughout the lattice and the formation of $Cu_{2-x-4y}Sn_ySe$ intermediates. Similarly to the case of
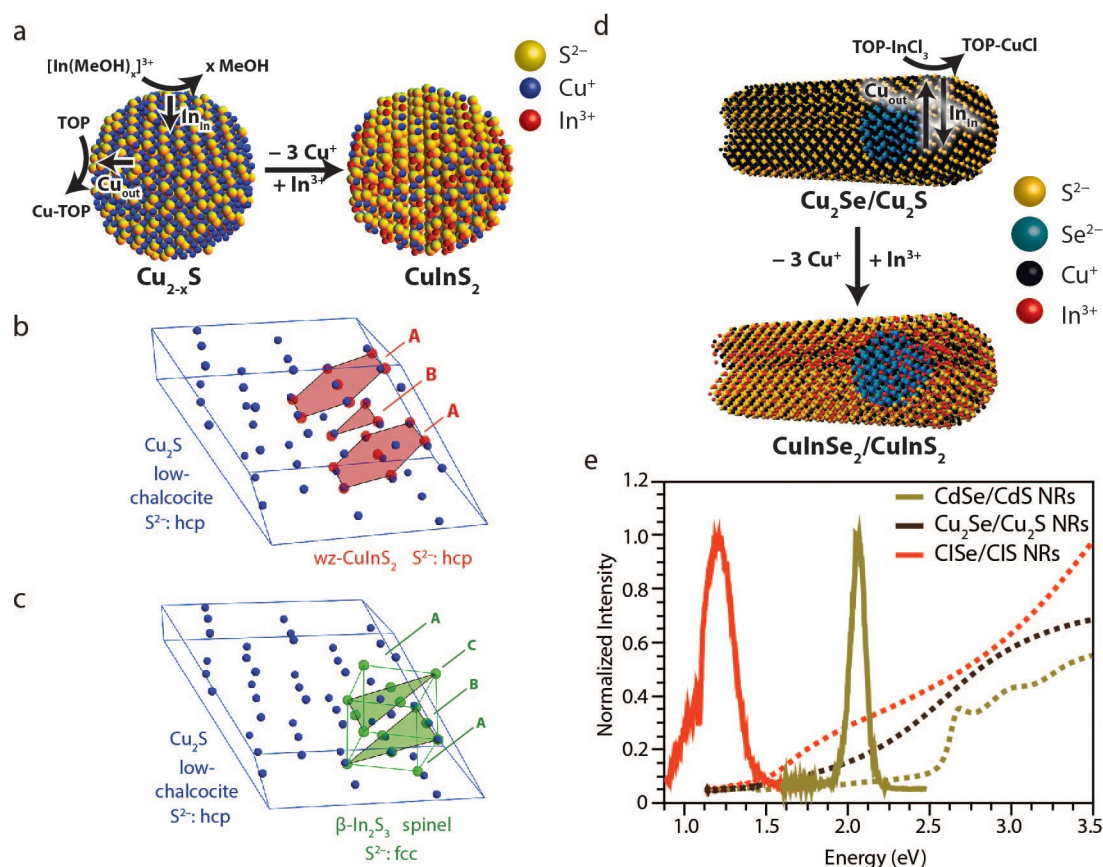

Figure 9. Formation of ternary CuIn chalcogenide NCs and hetero-NCs by partial, self-limited cation exchange in template $Cu_{2-x}S$ NCs. a) Schematic illustration of the elementary kinetic steps involved in conversion of $Cu_{2-x}S$ NCs into $CuInS_2$ NCs by Cu^+ for In^{3+} cation exchange. b) Comparison of the anionic sublattice of low-chalcocite $Cu_{2-x}S$ with wurtzite CIS, showing that the anionic sublattice of low-chalcocite $Cu_{2-x}S$ (blue spheres) is compatible with wurtzite CIS (red spheres), as both anionic sublattices have a hcp arrangement. c) Comparison of low-chalcocite unit cell (blue spheres) with In_2S_3 (green spheres). The spinel In_2S_3 structure has an fcc anionic sublattice, in which layer C has to dislocate by 58% of a S–S distance to fit in the low-chalcocite lattice. d) Schematic representation of In^{3+} for Cu^+ partial CE reaction with the use of a stoichiometric TOP–$InCl_3$ complex acting as both the Cu-extracting and In-incorporation agents, thereby effectively coupling the in- and outgoing diffusion rates. e) In this way, near-IR PL from ternary dot core–rod shell $CuInSe_2/CuInS_2$ heteronanorods is obtained by using CdSe/CdS heteronanorods with PL in the visible region as template in a sequential CE pathway. The panels were adapted with permission from Ref. [82] (panels a–c, Copyright 2015 American Chemical Society) and [78] (panels d,e; Copyright 2015 American Chemical Society).

CIS formation from $Cu_{2-x}S$ template NCs discussed above,[78,82] the Sn^{4+} for Cu^+ CE reaction is also self-limited due to the stable crystal structures of $Cu_{2-x}Se$ (hcp), Cu_2SnSe_3 (hcp), and $SnSe_2$ (fcc).[116]

3.2.2. Heteronanocrystals and Alloys Based on Ternary Copper Chalcogenides

The PL efficiency of colloidal NCs of semiconductors can be improved by growing a shell of another wide bandgap semiconductor.[1] This passivates surface traps and confines the photoexcited carriers to the core, which thereby protects the NC against oxidation and other unwanted nonradiative relaxation pathways.[1] Suitable wide bandgap semiconductors for heteroepitaxial shell growth on ternary CIS NCs are ZnS and CdS. Several groups have investigated the overgrowth of ZnS and CdS on CIS cores,[97,98] and in all cases a blueshift in the PL has been observed.[97,98] This blueshift has been explained by either alloying of the CIS NC core with the shell cations[97] or etching of the CIS core prior to shell overgrowth.[98] The occurrence of alloying during shell growth can be explained by the relatively small lattice mismatch between chalcopyrite CIS and zinc blende ZnS (1.6%) and the small radius of Zn^{2+}, which results in fast diffusion of the incoming cation into the CIS lattice. The resulting alloyed CIZS NCs do show enhancement in the PL quantum yield, which renders them promising materials for implementation into lighting devices or as luminescent probes for bioimaging applications[91,92] (see Section 3.3). The overgrowth of a shell of a different semiconductor can also be used to control the carrier localization regime in the hetero-NC (i.e. type I, type $I^{1/2}$, or type II),[1] which thereby allows the exciton radiative lifetimes, exciton–phonon coupling strength, and spectral characteristics (i.e. peak position, bandwidth, Stokes shift) of colloidal hetero-NC to be tailored.[117–119] This has been extensively investigated for the prototypical case of heteroNCs based on Cd chalcogenides and other II–VI materials[1] but has yet to be addressed for Cu chalcogenide based materials.

3.3. Properties and Potential Applications of Ternary Copper Chalcogenide Nanocrystals

3.3.1. Optical Properties of Ternary Copper Chalcogenide Nanocrystals

The optical properties of ternary copper chalcogenide NCs render them interesting materials for several applications (e.g. light-emitting diodes, luminescent solar concentrators, bioimaging; see Sections 3.3.3–3.3.5). The most investigated compositions are copper indium chalcogenide NCs ($CuInA_2$ NCs; A = S, Se, CIS and CISe), which have been shown to exhibit tunable PL from the visible region to the near-IR region (Figure 10). As will be discussed below, the wide tunability reported for the optical properties of CIS and CISe NCs is only partially due to quantum confinement effects (exciton Bohr radii are 4.1 and 7.5 nm for CIS and CISe,[11,120] respectively); this is in striking contrast with the II–VI binary analogues, which have been instrumental in the discovery and understanding of quantum confinement effects in semiconductor nanocrystals.[1]

The first important difference between binary II–VI and IV–VI compounds and ternary Cu III–VI compounds is that the former do not tolerate significant off-stoichiometry, whereas the latter can easily accommodate large deviations (a few percentage points) from the ideal chemical formula $CuXA_2$, both in the Cu/X ratio and in the $2A/[Cu+3X]$ ratio.[121–124] As a result, bulk CIS crystals have a very rich defect structure and can be grown both n-type (In excess) or p-type (S excess) and can be nonstoichiometric, even if the melt has the ideal composition because the homogeneity region at room temperature spans from 50 to 52 mol% In_2S_3.[121] This extreme tolerance to off-stoichiometry is also manifested by the existence of a series of compounds with different Cu/In/A ratios ($CuIn_5A_8$, $CuIn_3A_5$, $Cu_2In_4Se_7$, $Cu_3In_5Se_9$), which are absent in II–VI compounds and their alloys.[124] The rich defect structure of $CuInA_2$ has been explained by theoretical studies, which show that the formation energies of native defects are much lower in ternary $CuInA_2$ compounds than in the binary II–VI analogues
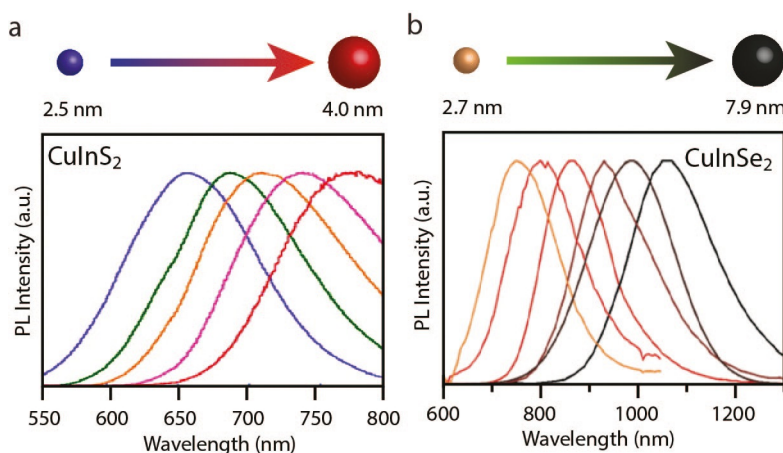

Figure 10. Tunable PL in ternary $CuInS(e)_2$ NCs. a) $CuInS_2$ nanocrystals of sizes varying between 2.5 and 4.0 nm show PL band positions between 650 and 800 nm. b) $CuInSe_2$ nanocrystals of sizes varying between 2.7 and 7.9 nm show PL band positions between 720 and 1080 nm. The panels were adapted with permission from Refs. [98] (panel a, Copyright 2011 American Chemical Society) and [105] (panel b, Copyright 2013 American Chemical Society).

(e.g. <2 eV for CISe and ≥ 6 eV for ZnSe).[124] The calculated formation energies for electrically neutral defect pairs such as $(2\,V_{Cu}^- + In_{Cu}^{2+})$ and $(2\,Cu_{In}^{2-} + In_{Cu}^{2+})$ are particularly low; they are even exothermic (-1.46 eV) under certain conditions (optimal chemical potential). It is noteworthy that the tolerance to off-stoichiometry becomes even larger at the nanoscale, as CIS NCs can be readily made with Cu/In ratios ranging from 0.3 to 2.9.[125]

Another crucial difference between ternary copper chalcogenides and binary II–VI semiconductors is the nature of the valence and conduction bands (VB and CB, respectively), which in II-VI semiconductors are, respectively, predominantly anionlike (the p orbitals of the group VI element) and cation-like (the s orbitals of the group II element) states.[126] In contrast, the upper VB in ternary copper chalcogenides is composed primarily of Cu 3d orbitals hybridized with the p orbitals of the group VI element, whereas the CB consists of Cu 4s orbitals with some mixing of p character from the chalcogen atoms.[126] This has a significant impact on the optical band gap of these materials, which becomes composition-dependent, as an increase in the Cu content pushes the VB top to higher energies and this thereby decreases the bandgap. This theoretical prediction is confirmed by a number of experimental observations, for which band gap reductions of up to 190 meV have been reported by increasing the Cu/In ratio from 0.9 to 2, accompanied by the development of a low-energy tail extending up to 200 meV below the band gap.[122,123]

Unlike nanocrystals of II–VI (e.g. CdSe or CdTe) and IV–VI (e.g. PbSe) semiconductors, CIS and CISe NCs typically present essentially featureless absorption spectra and do not exhibit a sharp first absorption transition, even for NCs sufficiently small to be in the quantum confinement regime. Moreover, a low-energy tail is usually observed. These characteristics may be due to size and shape inhomogeneities within the NC ensemble but are also likely to be an intrinsic property of CIS and CISe NCs, as improvements in the preparation methods have resulted in smaller size and shape dispersions but have not significantly narrowed the observed spectral linewidths.[11] As discussed above, CIS can easily accommodate stoichiometry devi-

ations. It is thus possible that ensembles of CIS, CIS/ZnS, or CIS/CdS will possess composition inhomogeneities, even if they are monodisperse in size and shape. The same reasoning can be applied to CISe NCs.

The PL of CIS and CISe NCs is also dramatically different from that observed for II–VI and IV–VI quantum dots and is characterized by a broad band (full width at half maximum ≈ 200–300 meV), a large "global" Stokes Shift (≈ 300 meV), and multiexponential PL decays with long decay constants (fast component with tens of nanoseconds, slow component with hundreds of nanoseconds).[11] The PL quantum yields (PL QYs) of bare CIS NCs are typically below 5–10%, whereas PL QYs as high as 70–85% have been reported for CIS/ZnS and CIS/CdS core–shell HNCs.[97,98] Interestingly, shell overgrowth makes the observed lifetimes even longer, as it reduces the contribution of the fast decay component. Despite a decade of research, the origin of these intriguing optical properties is not yet understood and is still under debate. The most often used model is that the PL of CIS NCs has the same origin as that of bulk CIS[11,127] and is thus due to a donor–acceptor pair recombination involving native point defects such as Cu_{In}, V_{In}, or V_{Cu} (Figure 11 a).[128,129] This model is consistent with the observation that the PL band position depends on the CIS NC composition (PL band shifts to shorter wavelengths with decrease in the Cu/In ratio[125]) and is based on the assumption that the defect structure of CIS does not change at the nanoscale. Under this assumption, and taking the concentrations of point defects determined for bulk CIS (namely, 1.6×10^{19} to 2×10^{20} cm^{-3}),[121] one can estimate that a CIS NC with a diameter as small as 3 nm could already contain between 0.14 and about $3\,V_{Cu}$–V_S pairs per NC. Nevertheless, this model fails to explain the size dependence of the PL energies, which follow the same trend as that observed for the absorption transitions, shifting to higher energies with decreasing NC size (Figure 10).[98,105] This requires that at least one of the carriers is quantized and delocalized over the whole NC.

To satisfy the requirement of at least one delocalized carrier, some studies propose that the PL of CIS NCs is due to radiative recombination of quantized VB hole states with electrons local-
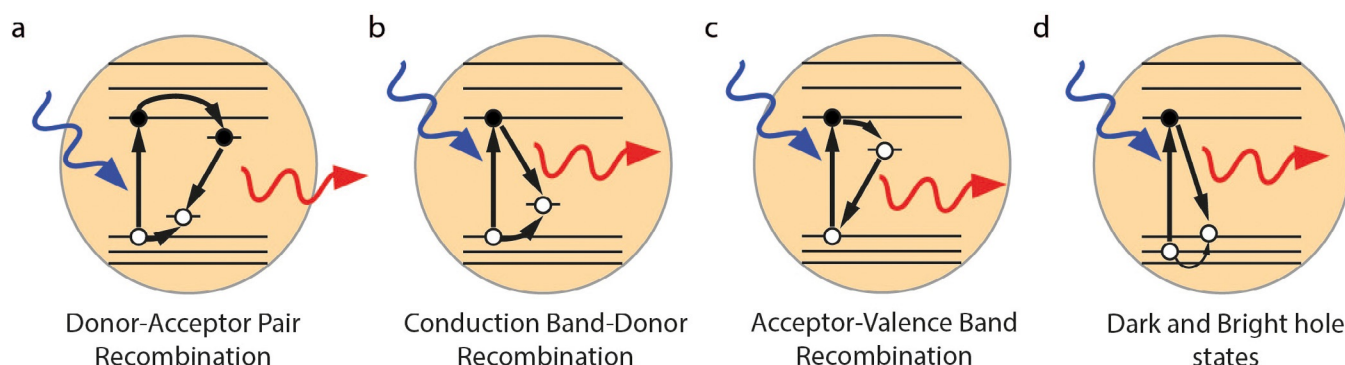

Figure 11. Possible recombination pathways in CuInS$_2$ nanocrystals. The origins of the intriguing optical properties of CuInS$_2$ NCs are not yet understood and are still under debate. a) The most often used model is that the PL of CIS NCs is due to a donor–acceptor pair recombination involving native point defects such as Cu$_{In}$, V$_{In}$, or V$_{Cu}$. b) Others have attributed the PL to recombination of quantized CB electron states with localized holes. c) Some studies propose that the PL of CIS NCs is due to radiative recombination of quantized VB hole states with electrons localized at native point defects. d) A recent theoretical paper by Efros and co-workers[133] proposes that the PL of CIS NCs is intrinsic and originates from the 1S(e)→1S(h) exciton transition.

ized at native point defects (Figure 11 c),[130, 131] whereas others attribute the PL to the recombination of quantized CB electron states with localized holes (Figure 11 b).[98, 132] The essential difference between the latter two studies is that Klimov and co-workers[98] assume that the hole is localized at native core defects, whereas Gamelin and co-workers[132] propose that the PL in CIS NCs is fundamentally different from that of bulk CIS, in the sense that the hole localization does not occur at native point defects but instead results from a strong hole–phonon coupling and large nuclear reorganization energies upon localization, which induces hole self-trapping at a regular Cu^+ ion (Figure 11 b). This model is thus based upon the assumptions that nanoscale CIS has a stronger hole–phonon coupling than bulk CIS and that native point defects are either no longer present in nanoscale CIS or only give rise to nonradiative recombination centers, in contrast with the bulk CIS. However, these assumptions have not yet been verified.

In a recent theoretical paper by Efros and co-workers,[133] yet one more model is proposed to explain the PL of CIS NCs: it is intrinsic and originates from the 1S(e)→1S(h) exciton transition (Figure 11 d), similarly to the prototypical cases of the II–VI and IV–VI QDs. This model is radically different from all the models discussed above, as it involves the recombination of quantized CB electron states with quantized VB hole states, which thus precludes the involvement of localized carriers. The large Stokes shift and long lifetimes are explained by the nature of the 1S(h) fine-structure states, of which the lowest emitting state is nominally a dark exciton and is separated by a large size-dependent energy gap from the upper fine-structure states. This model also explains the low-energy tail in the absorption spectra, which is assumed to originate from the emitting state itself. However, the broad bandwidths typically observed for both PL and band-edge absorption transitions are not addressed. The model also predicts a size-dependent Stokes shift, which has yet to be experimentally verified.

Understanding the size dependence of the absorption spectrum and of the absorption cross section (or extinction coefficient) of colloidal QDs is important from a fundamental viewpoint, but it is also crucial for their deployment in applications, as it allows the use of optical absorption spectroscopy to determine both the size and concentration of colloidal QDs. This has motivated worldwide research efforts over the last few decades on the size-dependent optical properties of colloidal QDs and has resulted in accurate sizing curves (i.e. empirical curves correlating the energy of the lowest exciton transition with the size of the QDs) and size-dependent molar extinction coefficients for a number of II–VI (i.e. CdS, CdSe, and CdTe),[134–137] and IV–VI (i.e. PbS, PbSe) QDs.[138, 139] Nevertheless, the situation for QDs of CIS and other ternary copper chalcogenides is still reminiscent of the early days of research on the archetypical II–VI QDs, for which large discrepancies between results from different groups were common.[134, 137]

To date, there are only two publications on the size-dependent molar extinction coefficient of the first exciton transition of CIS QDs,[140, 141] and they report widely different $\varepsilon(E1)$ values and size-dependent trends [i.e. $11430d^{2.147}$ with $d = 2$–6 nm and $(830 \pm 660)d^{3.7 \pm 0.6}$ with $d = 2.5$–5.1 nm in the works of Qin

et al.[140] and Booth et al.,[141] respectively]. Booth and co-workers have also investigated the size-dependent molar extinction coefficient at 3.1 eV for CIS QDs and CIS/ZnS core–shell QDs.[141] However, the observed size-dependency [i.e. $\varepsilon(E1) = (2123 \pm 1090)d^{3.8 \pm 0.3}$] is far stronger than would be theoretically expected, as the spectral density of states far above the band edge is no longer significantly affected by quantum confinement effects.[142] Therefore, the extinction coefficient per QD at energies far above the band edge should scale with the volume (i.e. d^3). This has been experimentally demonstrated for a number of QD compositions (e.g. CdSe,[134, 142] CdTe,[134] PbSe,[139] and InAs[143]).

These discrepancies can be attributed to inherent experimental difficulties associated with accurate determination of sizes, concentrations, and absorption band positions of colloidal QDs. This is a particularly challenging endeavor for CIS QDs, because the first absorption band is rather broad and is affected not only by size and shape dispersion, but also by composition inhomogeneities within the ensemble (see above). Moreover, CIS NCs that are sufficiently small to be in the quantum confinement regime (2–6 nm) are typically pyramidal in shape (e.g. see Figure 6), which introduces further uncertainties in the determination of the NC size. It is thus clear that more work is needed to determine the size dependence of the molar extinction coefficients of CIS QDs with an adequate degree of accuracy. It should also be noted that the molar extinction coefficients at energies far above the band edge are better suited for analytical purposes, because they are less sensitive to size and shape dispersions than those of the first exciton transition, which is strongly size (and shape) dependent.[134]

Future efforts should also be directed towards constructing reliable and accurate sizing curves for ternary copper chalcogenide QDs, as there are at present only three publications addressing this issue. The size dependence of the optical band gap has been experimentally investigated for pyramidal CIS NCs with diameters ranging from (3.0 ± 0.6) to (7.0 ± 1.4) nm[144] and for pyramidal and spherical CISe NCs with diameters ranging from (2.7 ± 0.5) to (7.9 ± 1.5) nm.[105] The size dependence of the optical band gaps of ternary $CuXA_2$ semiconductors (X = In, Ga; A = S, Se) has also been theoretically investigated by Omata and co-workers.[145]

Finally, ternary copper chalcogenide NCs can also sustain LSPR transitions if they possess a sufficiently high concentration of excess free carriers, similarly to the case of the binary $Cu_{2-x}A$ NCs discussed above (see Section 2.4.2). LSPR transitions, characterized by a broad absorption feature in the near-IR region, have been reported for CTS(e) NCs[146] and Cu-rich CIS NCs.[147]

3.3.2. Photovoltaic Applications

The reported bulk band gap of $CuInS_2$ at room temperature varies between 1.52 and 1.55 eV,[11] whereas the Se and Te analogues, $CuInSe_2$ and $CuInTe_2$, have reported bulk bandgaps of 1.01 and 0.97 eV, respectively.[11] $Cu(In,Ga)Se_2$ (CIGS) alloys have a band gap that can be tuned from 1.0 to 1.7 eV depending

on the Ga content.[46] The combination of suitable band gaps and large absorption coefficients has made ternary copper chalcogenides very attractive photoabsorbers for thin-film PV devices. In fact, CIGS thin-film PV devices hold the record for the highest device efficiency of all thin-film solar cells at just over 20%.[148] However, the fabrication of thin-film devices still involves expensive techniques (e.g. chemical vapor deposition), which hinders their widespread deployment. This has motivated intense research efforts into alternative manufacturing techniques. One promising approach to low-costing thin-film solar cells is to deposit the absorber layer by using a nanocrystal ink and a high-throughput method such as solution coating or printing.[7,8] In this way, the production process becomes much cheaper and easier to upscale. CIGS devices prepared from NC inks are still less efficient (i.e. 12% after high-temperature sintering) than those manufactured by using conventional techniques,[8] but the field is progressing very fast. The main factor limiting the performance of CI(S,Se) and CIGS NC solar cells, particularly if unsintered, is poor charge transport.[149] A recent study has shown that the carrier mobility and polarity of charge transport in films of $CuIn(Se,S)_2$ QDs can be postsynthetically tuned both by ligand exchange (i.e. exchanging the native DDT ligands by shorter ligands, such as 1,2-ethanedithiol) and by composition tailoring through cation exchange (Cd^{2+} leads to ambipolar behavior, whereas In^{3+} results in n-type mobility); this results in an increase in the mobilities by more than two orders of magnitude.[149]

Another possible low-costing PV device is the so-called dye-sensitized solar cell or Grätzel cells.[87,88,150,151] Colloidal semiconductor NCs have attracted increasing attention over the last decade as alternatives to organic dyes and metal complexes as sensitizers in Grätzel cells, and this has given rise to the so-called quantum-dot-sensitized solar cells (QDSSCs). Most of the work on QDSSCs has been done with the use of Cd or Pb chalcogenide QDs, but the combination of CIS/ZnSe alloyed core–shell NCs with TiO_2 nanoparticles coated with Cu_2S as a buffer layer has shown promising characteristics (Figure 12 a).[87] Indeed, Cd- and Pb-free QDSSCs with power conversion efficiencies of 7% have been recently realized by using CIS/ZnS alloyed core–shell NCs as sensitizers on TiO_2 mesoporous films (Figure 12 b).[88] In this way, heavy-metal-free QDSSCs can be achieved, which is beneficial for the large-scale deployment of these PV devices.

3.3.3. Light-Emitting Diodes

The size-tunable luminescence colors, high efficiency, and solution processability of colloidal QDs make them attractive materials for light-emitting devices (LEDs). Electrically driven colloidal quantum-dot light-emitting devices (QD-LEDs) have increased in external quantum efficiency from less than 0.01 to around 18% in the last 20 years, approaching a level of maturity that make them commercially viable.[5] Colloidal QDs have also been used as spectral converters in QD-enhanced displays and solid-state light sources, in which their PL is harnessed to
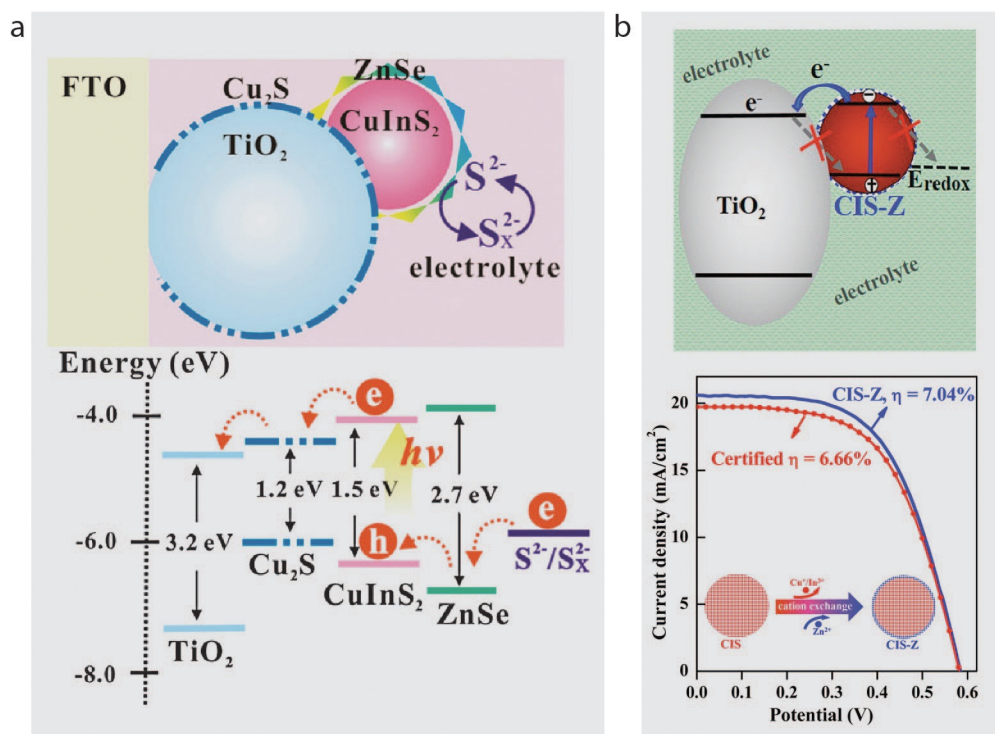

Figure 12. Quantum-dot-sensitized solar cells with CIS NCs as sensitizers. a) The electrons are effectively injected into the TiO_2 particles, whereas the hole is captured by the electrolyte. In this way, a photocurrent is generated. FTO=fluorine doped tin oxide. b) CIS NCs have been shown to be efficient sensitizers in QDSSCs, with a record efficiency of 7.04%. The panels were adapted with permission from Ref. [87] (panel a, Copyright 2012 The Royal Society of Chemistry) and [88] (panel b, Copyright 2014 American Chemical Society).

convert part of the emission of blue LEDs into other spectral colors, which thereby improves the color rendering index (CRI) and energy efficiency of the device. A recent example of this application is the use of QDs in combination with blue LEDs in the backlighting of high-resolution liquid-crystal televisions. Despite these recent advances, there are still a number of challenges that must be overcome before QD-LEDS and QD-enhanced light sources and displays become a widespread technology.[5] One of these challenges is the toxicity associated with Cd chalcogenides, which severely limits their use in consumer electronics.

CIS and other ternary copper chalcogenides have been extensively investigated in the last few years as potential replacements for Cd chalcogenides in LEDs, because they are inherently less toxic and also offer size-tunable luminescence colors, high efficiency, and solution processability. As discussed above, the PL of CIS is characterized by a broad bandwidth. This is a drawback for applications in full-color displays, as it precludes the production of high-purity colors with high efficiency. Nevertheless, a broad PL spectrum can be advantageous for indoor lighting, because a mix of different wavelengths over a large part of the visible spectrum can be easily obtained, which thereby provides a more natural white light. For example, green-emitting ($PL_{max} = 501$ nm) $AgInS_2$/ZnS and red-emitting ($PL_{max} = 606$ nm) CIS/ZnS alloyed core–shell NCs have been recently used as spectral down-converters in combination with a blue LED to produce warm white LEDs (CRI = 94–97) (Figure 13).[84] Extensive research has also been performed into ways to produce optically transparent composites of CIS NCs and polymers (including light-emitting conducting polymers).[85,86] One important question that has not yet been addressed for CIS NCs is the thermal quenching of its PL. Thermal quenching of QD PL is important for application in QD-LEDs and QD-enhanced LEDs, as in high-power LEDs for general-lighting applications, temperatures as high as 150–200 °C may be reached in the layer applied on top of the blue LED.[152]
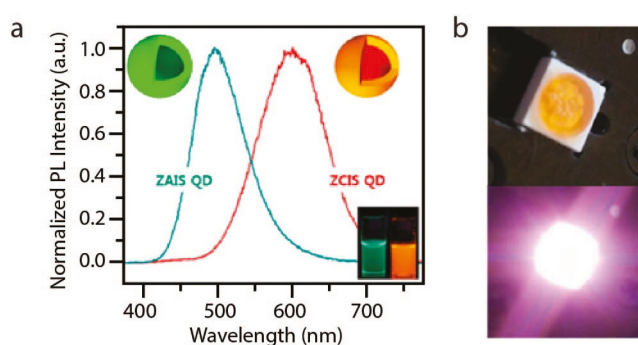

Figure 13. Ternary Cu chalcogenide NCs for lighting applications. a) Green-emitting ($PL_{max} = 501$ nm) $AgInS_2$/ZnS and red-emitting ($PL_{max} = 606$ nm) CIS/ZnS alloyed core–shell NCs are useful spectral down converters in combination with blue LEDs to produce warm white light (CRI = 94–97). b) Photographs of LED produced with ternary Cu chalcogenide NCs. Adapted with permission from Ref. [84], Copyright 2015 American Chemical Society.

3.3.4. Luminescent Solar Concentrators

Luminescent solar concentrators (LSCs) consist of thin transparent sheets or slabs, typically made of polymers, in which luminescent species (luminophores) are dispersed.[153] Direct and diffuse sunlight entering the LSC is absorbed by the luminophores and is re-emitted at longer wavelengths. A large fraction of the emitted light is trapped and waveguided by total internal reflection to the edges of the LSC, where it is converted into electricity by long and slim solar cells. In this way, LSCs effectively concentrate the incident sunlight onto the solar cells, which thereby boosts their photocurrent output and generates more power per area of deployed PV material. LSCs are particularly attractive for the urban environment, as they can easily be integrated into facades and semitransparent windows; this thereby converts them into energy-generation units, capable of harvesting both direct and diffuse light, while fulfilling a number of other structural and architectural functions.[154]

Despite their promise, LSCs have not yet become commercially viable, as their power efficiencies are still too low. The power efficiency of an LSC is determined by the product of the efficiency of the attached solar cells and the optical efficiency of the LSC plate itself. The most convenient metric to allow comparison between different LSC devices is thus the optical power efficiency. The optical efficiency of LSCs is limited by a number of loss mechanisms, of which many are related to the characteristics of the luminescent species (PL QYs, PL spectra, absorption cross section, Stokes shift). The development of LSCs has thus been stalled by the lack of suitable luminophores.

Colloidal QDs are promising luminophores for LSCs, because they have very broad absorption spectra (any photon with energy equal to or higher than the band edge is absorbed), large absorption cross sections, narrow and size-tunable PL spectra, and potentially high PL QYs. Nevertheless, their utilization in LSCs has been hindered by the small Stokes shifts of the commonly available compositions, which results in large reabsorption losses. It has been recently demonstrated that type II CdTe/CdSe HNCs can decrease the reabsorption losses in LSCs to negligible levels, due to their large Stokes shifts.[152] However, the applicability of these HNCs is severely limited by the toxicity of Cd. Ternary copper chalcogenides, such as CIS and CISe, have been proposed as nontoxic alternatives, as they are also characterized by large Stokes shifts.[82,89,90] This potential has been recently validated by the fabrication of a LSC plate ($12 \times 12 \times 0.3$ cm^3) with an optical efficiency of 3.2% at $\lambda = 960$ nm by using $CuIn(S,Se)_2$/ZnS core–shell QDs (PL QY: 40%) embedded into poly(lauryl methacrylate) plates.[89] This optical efficiency is still lower than that predicted by other authors for similar devices by using ray-tracing models (6.7% for CISe QDs emitting at $\lambda = 900$ nm with PL QY = 75%, $10 \times 10 \times 1$ cm^3 plate[155]), probably due to the relatively low PL QY of the QDs used to fabricate the device reported in Ref. [89].

3.3.5. Bioimaging Applications

The unique optical properties of colloidal QDs have turned them into an important class of luminescent contrast agents and probes for in vitro and in vivo biomedical imaging.[6] In contrast to conventional organic dyes and fluorescent proteins, QDs possess very broad absorption spectra, narrow PL bands, large absorption cross sections, high PL QYs (and hence superior brightness), and long PL lifetimes, and additionally, they are highly resistant to photobleaching.[6, 156, 157] Furthermore, their PL can be tuned from the green to the near-IR biological windows (i.e. I-BW from $\lambda = 650$–950 nm and II-BW from $\lambda = 1000$–1350 nm)[158] by proper choice of the composition and size.[6, 156, 157] This combination of properties has been translated into longer observation times, higher sensitivity, multiplexed detection (i.e. multiple PL colors upon a single excitation wavelength), and background-free imaging (time-gated detection allows faster PL from biological tissue to be discarded).[6, 156, 157] Another important advantage of QDs is that they can be used as multimodal imaging probes, in which two or more imaging modalities are combined (e.g. magnetic resonance imaging and optical, positron emission tomography and optical, etc.).[6, 159, 160]

Nevertheless, the widespread use of QDs as biomedical labels, especially for application in humans, is still severely hampered by the intrinsic toxicity of the heavy-metal elements present in the currently used QDs (e.g. CdSe-based core–multishell QDs, PbS- and PbSe-based core–shell QDs). This has motivated an intense search for alternative QD compositions, amongst which CIS stands out as a very promising one, because it meets all the requirements for application as a biomedical contrast agent and is potentially less toxic. In comparison to conventional Cd- and Pb-based QDs, CIS QDs also have the advantage of an even larger absorption cross section. Moreover, their spectral tunability is unsurpassed by any other semiconductor compound, as they can be made to emit anywhere from orange to the near-IR biological windows I and II, spanning a spectral window that covers the PL tunability of CdSe QDs (visible), CdTe/CdSe (near-IR BW-I), and PbS (near-IR BW-II).

In a recent study, Chen and co-workers have investigated the toxicity and chemical stability of CIS/ZnS QDs capped with hydrophilic O-carboxymethylchitosan ligands.[91] No signs of toxicity have been observed upon incubation of these particles with cancer cells (HeLA and OECM-1) for 72 h (90% of the cells were still viable). Furthermore, X-ray absorption near edge structure (XANES) studies confirm the chemical stability of the particles in the digestive system of the model organism C. elegans in the 12 to 72 h time range.[91] The reduced toxicity of CIS/ZnS QDs and their suitability for in vivo imaging in the near-IR BW-I have also been demonstrated in a study using them for sentinel lymph node imaging in live mice.[161] Near-IR-emitting ($\lambda = 760$ nm) CIS QDs have also been used for in vivo imaging of brain tumors in a mouse model.[162] Guo and co-workers[92] have used a different approach to image tumor cells, by incorporating radioactive Cu [^{64}Cu] in CIS/ZnS NCs (Figure 14). In this way, they have obtained self-illuminating NCs by Cerenkov resonance energy transfer (CRET), and these
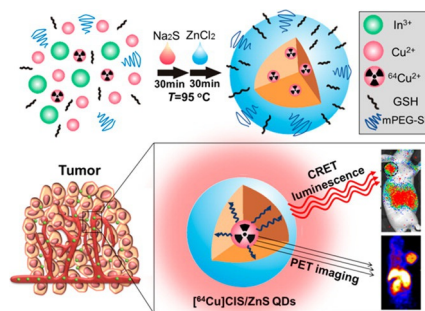

Figure 14. Ternary Cu chalcogenide NCs for bioimaging applications. By incorporating radioactive Cu [^{64}Cu] in CIS/ZnS NCs, self-illuminating NCs are obtained by Cerenkov resonance energy transfer, and they have been used as bimodal (optical and positron emission tomography) labels for in vivo imaging of tumors in mice. mPEG = methoxypoly(ethylene glycol). Adapted with permission from Ref. [92], Copyright 2015 American Chemical Society.

NCs have been used as bimodal [optical and positron emission tomography (PET)] labels for in vivo imaging of tumors in mice.[92] The reduced toxicity of the QDs has been demonstrated by cell viability studies, for which no effects have been observed after 24 h incubation of 100 µg mL^{-1} solution. Furthermore, no abnormalities or lesions have been observed in any major mice organs 2 and 14 days after injection.[92] The studies reviewed above, and many others, clearly illustrate the potential of CIS-based QDs for bioimaging applications. Nevertheless, the field is still in its infancy and, therefore, many new exciting developments can be expected in the coming years. For example, Förster resonance energy transfer (FRET) and multimodal imaging studies involving CIS QDs are still scarce in contrast to conventional heavy-metal based QDs. Moreover, sophisticated techniques, such as super-resolution microscopy and single-particle tracking have yet to be applied to CIS QDs.

4. Quaternary Copper Chalcogenides

Quaternary copper chalcogenides (Cu$_2$ II–IV–VI$_4$; II = Zn, Cd; IV = Ge, Sn, Si; VI = S, Se) have attracted much attention due to the many possibilities they offer in terms of varying their chemical composition, which thereby allows the material band gap (0.8 to 3.3 eV) and functionality to be optimized.[163–165] These materials are thus promising for nonlinear optics, LEDs, and photovoltaics. Specifically, Cu$_2$ZnSnS$_4$ (CZTS) has drawn much attention in recent years in the search for inexpensive, earth-abundant, and nontoxic photoabsorbers for thin-film solar cells (see Section 4.3.1).[12, 166] CZTS can be seen as an analogue of CIGS, in which the rare and expensive group III elements (i.e. In and Ga) are replaced by earth-abundant and nontoxic elements (see Section 4.1), while keeping the high stability, large absorption coefficient, and ideal band gap (1.5 eV). CZTS has also been recently proposed as a promising material for high-temperature thermoelectric harvesting.[167]

4.1. Crystal Structure of Quaternary Copper Chalcogenides

The most common crystal structures for quaternary copper chalcogenides are kesterite,[168] stannite,[169] and wurtzite,[170]

which differ both in the cation positions (kesterite vs. stannite) and in the anion distribution within the lattice (kesterite/stannite vs. wurtzite, see Figure 5).[94] The wurtzite structure is less stable at room temperature for bulk materials but can be obtained for nanocrystals, depending on the synthesis conditions (see Section 4.2).

4.2. Colloidal Synthesis of Quaternary Copper Chalcogenide Nanocrystals

As mentioned above (Section 3.3.2), colloidal NC inks offer an interesting alternative route to inexpensive thin-film solar cells.[63,64,171,172] This prospect has provided most of the motivation driving the development of synthesis protocols for monodisperse colloidal NCs of CZTS and related materials,[46,61,63,64,173–175] as a large size and shape distribution is detrimental to the quality of the NC film obtained from NC inks. The colloidal synthesis of size- and shape-controlled quaternary Cu chalcogenide NCs is particularly challenging, because multiple precursor reactivities must be balanced to achieve nucleation and growth of a quaternary composition.[176,177] This strongly limits the morphologies that can be obtained.[168,178–181] Typically, mainly large NCs with a broad size and shape distribution have been synthesized (Figure 15b,c). However, the synthesis protocols have become more mature over the last few years, and this has resulted in well-defined spherical NCs with a narrow size distribution[182] (Figure 15a) and monodisperse bullet-shaped nanorods[180,183] (Figure 15d).

Another important parameter in the synthesis of quaternary NCs is the crystal structure of the materials obtained. It has been shown that the crystal structure of the final NCs is strongly influenced by the choice of the anion precursor.[176,184] For example, the use of elemental anion sources results in the zinc blende derivative (kesterite or stannite), whereas NCs with the wurtzite structure are obtained if DDT or bis(dimethylsilyl)-sulfide is used as the sulfur precursor.[183] A recent study by Ryan and co-workers[180] has investigated the occurrence of polytypism between wurtzite and zinc blende phases in $Cu_2ZnSn(S,Se)_4$ NCs, and it has been shown that the choice of solvents, surfactants, and precursors, and the way in which they are introduced, are key factors that control the shape of the NCs from dots to ellipsoids, arrows, and rods. Further, the authors have shown that the shape evolution is dictated by independently controlling the growth rates of either the wurtzite or the zinc blende regions in the polytypic system, extending the methodology to the preparation of single-phase wurtzite CZTSSe nanorods.[180]

The growth mechanism of colloidal CZTS nanoplatelets has been recently investigated with TEM and Raman spectroscopy (Figure 16).[185] In the study, it is shown that the disparity in the reactivities of the different metal precursors causes the NCs to grow in a stepwise fashion: Cu_2S NCs nucleate and grow first, which provides seeds into which Sn^{4+}, and subsequently Zn^{2+}, diffuse.[185] The diffusion is accompanied by reaction with the sulfur precursor (e.g. DDT), which effectively leads to incorporation of $[SnS_2]$ and $[ZnS]$ units in the growing NC. This results

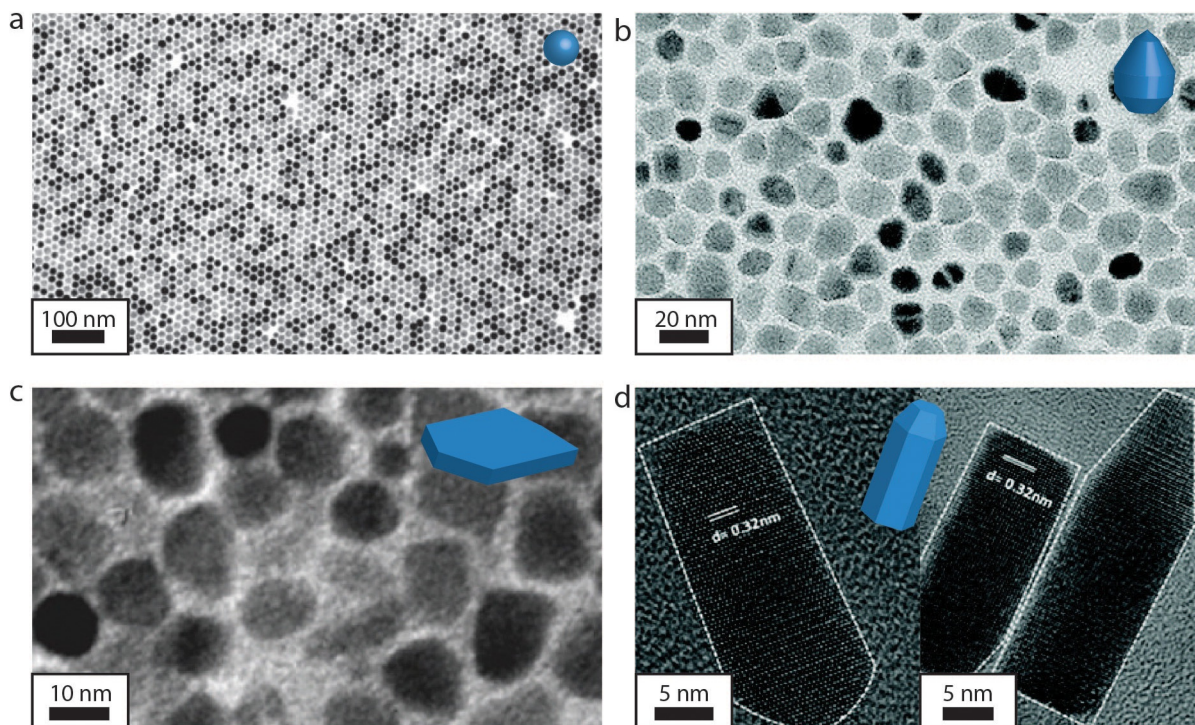**Figure 15.** Quaternary Cu_2ZnSnS_4 (CZTS) NCs with various sizes and shapes. TEM images of a) spherical CZTS NCs, b) anisotropic egg-shaped CZTS NCs, c) CZTSSe nanoplatelets, and d) wurtzite CZTS nanorods. The panels were adapted with permission from Refs. [182] (panel a, Copyright 2014 American Chemical Society), [65] (panel b, Copyright 2009 American Chemical Society), [189] (panel c, Copyright 2014 American Chemical Society), and [183] (panel d, Copyright 2012 American Chemical Society).
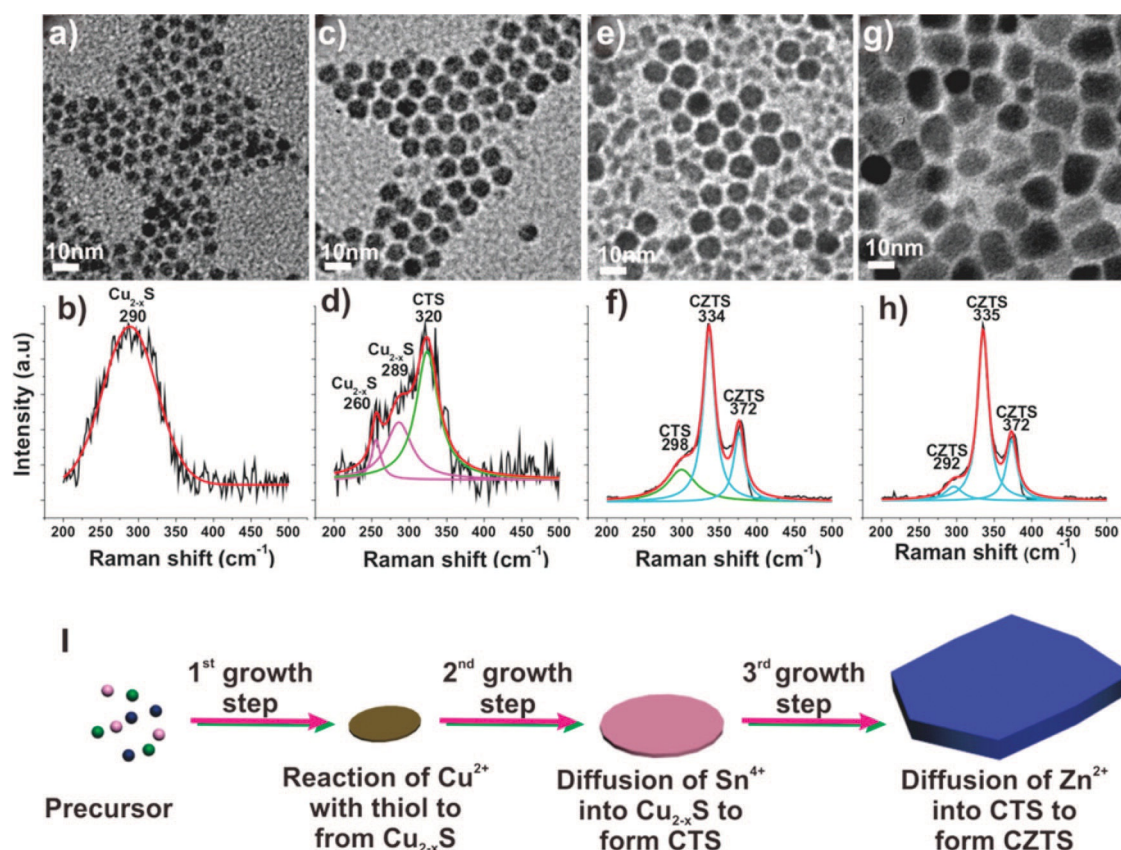
Figure 16. Growth of quaternary CZTS nanocrystals. a–d) First, $Cu_{2-x}S$ NCs nucleate as small quasispherical clusters. e,f) In the second step, Sn^{4+} diffuses in, resulting in anisotropic CTS nanoplatelets. g,h) In the third step, Zn^{2+} finally diffuses in, causing a large increase in lateral dimensions. i) Schematic representation of the steps involved in the growth of quaternary CZTS nanoplatelets. Reproduced with permission from Ref. [185], Copyright 2014 American Chemical Society.

in particles with broadened size and shape distributions. We note that this growth mechanism is similar to that proposed for the formation of Cu_2SnS_3 NCs[112] and CIS wurtzite nanorods[101] (see Section 3.2 and Figure 7), for which Cu_2S NCs nucleate first and act as seed particles into which the second cation (Sn^{4+} or In^{3+}) is subsequently incorporated as [MS_x] units, and this leads to growth of NCs with a ternary composition.

The quest for control over the size and shape of NCs of quaternary copper chalcogenides has been driven not only by the requirements of NC inks for printable thin-film PV cells, but also by the desire to make NCs sufficiently small to be in the quantum confinement regime. This is of great fundamental interest and is also relevant for potential applications such as LEDs and multijunction QD solar cells, as it allows quantum confinement effects to be exploited to tune the optoelectronic properties of the NCs. Nevertheless, from this perspective, the synthesis of NCs of quaternary copper chalcogenides is still largely underdeveloped, as there is to date only one report on CZTS NCs sufficiently small to exhibit quantum confinement effects (i.e. 2 nm and 2.5 nm in diameter, exciton Bohr diameter is estimated to be 5–6 nm).[186] It is noteworthy that no PL has ever been reported for CZTS NCs at room temperature, regardless of their size, in contrast to NCs of the related ternary copper chalcogenides (e.g. CIS and CISe), which typically exhib-

it size-tunable PL (see Section 3.3.1). In fact, CZTS NCs have only been observed to luminesce at low temperatures (20 K), and even then with relatively low efficiencies.[187] In the study performed by Ryan and co-workers, the PL of CZT(S,Se) NCs ($\approx$11 nm diameter) at 20 K was observed to shift to lower energies and to become stronger and narrower with an increase in the Se content.[187] The PL energies are reported to follow the same trend as that of the composition-dependent bandgaps, and this has led the authors to assume the PL is due to near band-edge emission.[187] PL is also unusual for bulk CZTS crystals and has been reported only once for slightly S-poor crystals at 25 K and assigned to donor–acceptor recombination.[188]

4.2.1. Alternative Synthesis Routes to Quaternary Copper Chalcogenide Nanocrystals

As discussed above (Sections 2.4.3 and 3.2.1), cation exchange (CE) has emerged as a powerful and versatile tool to circumvent synthetic limitations and has yielded a variety of novel colloidal NCs, with sizes, shapes, and/or compositions that would otherwise not be attainable. Accordingly, CE has also been successfully used to obtain NCs of quaternary copper chalcogenides. For example, a one-pot synthesis approach has been developed to convert $Cu_2(Se,S)$ nanoplatelets into
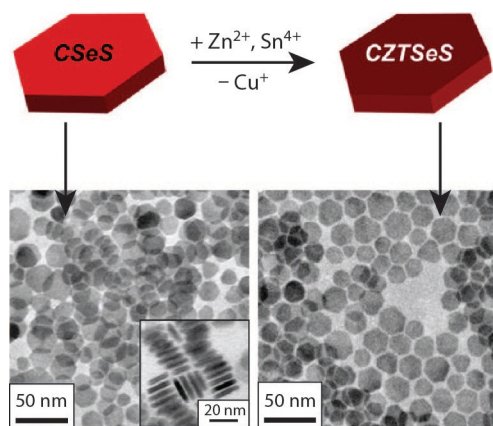
Figure 17. Cation-exchange reactions as a possible pathway to produce well-defined CZTS(e) NCs. Cation-exchange reaction in Cu$_2$(Se,S) (CSeS) nanoplatelets, resulting in Cu$_2$ZnSn(Se,S)$_4$ (CZTSeS) hexagonal nanoplatelets with size and shape preservation. Adapted with permission from Ref. [189], Copyright 2014 American Chemical Society.

Cu$_2$ZnSn(Se,S)$_4$ nanoplatelets with size and shape preservation by using in situ CE reactions (Figure 17).[189] It is interesting to note that in situ CE reactions can be distinguished from the stepwise growth mechanism discussed above (Cu$_{2-x}$S NCs nucleate first and serve as seeds into which the second and third cations are subsequently incorporated as [MS] units), because the size and shape of the parent NC is preserved into the product NC, that is, no net growth occurs.

4.3. Potential Applications of Quaternary Copper Chalcogenide Nanocrystals

4.3.1. Photovoltaic Applications

As mentioned above, CZTS has attracted increasing attention as an inexpensive alternative to CIGS as a photoabsorber in thin-film solar cells, as it lacks the rare and expensive group III elements but also has high stability, large absorption coefficient, and ideal band gap (1.5 eV).[63, 147, 166, 190] The efficiency of CZT(S,Se) thin-film PV devices (i.e. 12.6%)[191] is still lower than those of CIGS (20%) and CdTe (16.7%) but is already higher than that of amorphous silicon (10%).[8] However, the fabrication techniques used to manufacture CZT(S,Se) thin films are still expensive (vacuum deposition) or rely on the use of toxic and unstable chemicals such as hydrazine. This has motivated extensive research into the development of size- and shape-controlled colloidal CZTS NCs for use in NC inks (see Section 4.2). The last few years have witnessed great progress in that direction, and many groups have already reported device efficiencies of up to 7% for CZT(S,Se) [or CZ(Sn,Ge)S] devices prepared from NC inks.[8, 174, 192] A recent work has investigated the impact of NC size and size distribution, average composition, and composition heterogeneity in the properties of CZT(S,Se) thin-film devices prepared from CZTS NC inks followed by selenization and sintering at 500 °C.[193] The authors conclude that longer NC synthesis times lead to more efficient devices, probably due to larger crystallite domain sizes after sintering. This implies that further progress will require the development of grain-boundary passivation techniques or NC synthesis and sintering methods that lead to better grain growth and more homogeneous inks.[193]

5. Summary and Outlook

There have been a number of recent advances in the synthesis of colloidal nanocrystals of Cu chalcogenides that have greatly improved the control of the size, shape, and composition of the resulting nanomaterials. In this respect, the development of topotactic cation-exchange protocols has been instrumental in circumventing the limitations inherent to the synthesis of nanocrystals of multinary compounds. The availability of high-quality materials has in turn boosted the understanding of the properties of Cu chalcogenide based NCs and hetero-NCs and has already been translated into improved devices and novel applications. There remain, however, many fundamental questions to be answered, particularly regarding the optoelectronic properties of ternary and quaternary copper chalcogenide nanocrystals. The investigation of Cu chalcogenide based hetero-NCs is particularly interesting, as this field is still in its infancy, primarily due to the lack of suitable materials. However, this hindrance has been recently lifted by the development of sequential cation-exchange protocols that allow the topotactic conversion of template Cd-based hetero-NCs into the ternary copper chalcogenide analogues. It is likely that further advances in this direction will open up a route toward a wide variety of ternary and quaternary Cu chalcogenide hetero-NCs with tailored sizes, shapes, compositions, and heteroarchitectures, and this may prove beneficial for a number of existing and novel technologies.

[1] C. d. M. Donegá, *Chem. Soc. Rev.* **2011**, *40*, 1512.
[2] C. Bouet, B. Mahler, B. Nadal, B. Abecassis, M. D. Tessier, S. Ithurria, X. Xu, B. Dubertret, *Chem. Mater.* **2013**, *25*, 639.
[3] O. Chen, J. Zhao, V. P. Chauhan, J. Cui, C. Wong, D. K. Harris, H. Wei, H.-S. Han, D. Fukumura, R. K. Jain, M. G. Bawendi, *Nat. Mater.* **2013**, *12*, 445.
[4] V. I. Klimov, S. A. Ivanov, J. Nanda, M. Achermann, I. Bezel, J. A. McGuire, A. Piryatinski, *Nature* **2007**, *447*, 441.
[5] Y. Shirasaki, G. J. Supran, M. G. Bawendi, V. Bulović, *Nat. Photonics* **2013**, *7*, 13.
[6] K. D. Wegner, N. Hildebrandt, *Chem. Soc. Rev.* **2015**, *44*, 4792.
[7] C. N. Bucherl, K. R. Oleson, H. W. Hillhouse, *Curr. Opin. Chem. Eng.* **2013**, *2*, 168.
[8] C. J. Stolle, T. B. Harvey, B. A. Korgel, *Curr. Opin. Chem. Eng.* **2013**, *2*, 160.
[9] Y. Zhao, C. Burda, *Energy Environ. Sci.* **2012**, *5*, 5564.

[10] S. Goel, F. Chen, W. Cai, *Small* **2014**, *10*, 631.

[11] J. Kolny-Olesiak, H. Weller, *ACS Appl. Mater. Interfaces* **2013**, *5*, 12221.

[12] D. Aldakov, A. Lefrançois, P. Reiss, *J. Mater. Chem. C* **2013**, *1*, 3756.

[13] J. M. Luther, P. K. Jain, T. Ewers, A. P. Alivisatos, *Nat. Mater.* **2011**, *10*, 361.

[14] A. L. Abdelhady, K. Ramasamy, M. A. Malik, P. O'Brien, S. J. Haigh, J. Raftery, *J. Mater. Chem.* **2011**, *21*, 17888.

[15] T. Kuzuya, Y. Tai, S. Yamamuro, K. Sumiyama, *Sci. Technol. Adv. Mater.* **2005**, *6*, 84.

[16] C. M. Hessel, V. P. Pattani, M. Rasch, M. G. Panthani, B. Koo, J. W. Tunnell, B. A. Korgel, *Nano Lett.* **2011**, *11*, 2560.

[17] S. Wang, A. Riedinger, H. Li, C. Fu, H. Liu, L. Li, T. Liu, L. Tan, M. J. Barthel, G. Pugliese, F. De Donato, M. Scotto D'Abbusco, X. Meng, L. Manna, H. Meng, T. Pellegrino, *ACS Nano* **2015**, *9*, 1788.

[18] D. C. Reifsnyder, X. Ye, T. R. Gordon, C. Song, C. B. Murray, *ACS Nano* **2013**, *7*, 4307.

[19] M. Sigman, A. Ghezelbash, *J. Am. Chem. Soc.* **2003**, *125*, 16050.

[20] X. Li, H. Shen, J. Niu, S. Li, Y. Zhang, H. Wang, L. S. Li, *J. Am. Chem. Soc.* **2010**, *132*, 12778.

[21] X. Li, M. Wang, H. Shen, Y. Zhang, H. Wang, L. S. Li, *Chemistry* **2011**, *17*, 10357.

[22] W. Li, A. Shavel, R. Guzman, J. Rubio-Garcia, C. Flox, J. Fan, D. Cadavid, M. Ibáñez, J. Arbiol, J. R. Morante, A. Cabot, *Chem. Commun.* **2011**, *47*, 10332.

[23] A. Tang, S. Qu, K. Li, Y. Hou, F. Teng, J. Cao, Y. Wang, Z. Wang, *Nanotechnology* **2010**, *21*, 285602.

[24] W. van der Stam, Q. A. Akkerman, X. Ke, M. A. van Huis, S. Bals, C. de Mello Donega, *Chem. Mater.* **2015**, *27*, 283.

[25] D. J. Chakrabarti, D. E. Laughlin, *Bull. Alloy Phase Diagrams* **1983**, *4*, 254.

[26] JCPDS cards 00-034-0171 klockmannite, 01-071-0045 umangite, 00-006-0680 berzelianite, 01-071-4325 bellidoite.

[27] H. Shen, H. Wang, H. Yuan, L. Ma, L. S. Li, *CrystEngComm* **2012**, *14*, 555.

[28] S. Deka, A. Genovese, Y. Zhang, K. Miszta, G. Bertoni, R. Krahne, C. Giannini, L. Manna, *J. Am. Chem. Soc.* **2010**, *132*, 8912.

[29] V. Lesnyak, R. Brescia, G. C. Messina, L. Manna, *J. Am. Chem. Soc.* **2015**, *137*, 9315.

[30] H. Li, R. Brescia, M. Povia, M. Prato, G. Bertoni, L. Manna, I. Moreels, *J. Am. Chem. Soc.* **2013**, *135*, 12270.

[31] W. Li, R. Zamani, P. Rivera Gil, B. Pelaz, M. Ibáñez, D. Cadavid, A. Shavel, R. A. Alvarez-Puebla, W. J. Parak, J. Arbiol, A. Cabot, *J. Am. Chem. Soc.* **2013**, *135*, 7098.

[32] C. Han, Z. Li, W. Li, S. Chou, S. Dou, *J. Mater. Chem. A* **2014**, *2*, 11683.

[33] Y. Xie, A. Riedinger, M. Prato, A. Casu, A. Genovese, P. Guardia, S. Sottini, C. Sangregorio, K. Miszta, S. Ghosh, T. Pellegrino, L. Manna, *J. Am. Chem. Soc.* **2013**, *135*, 17630.

[34] Y. Xie, L. Carbone, C. Nobile, V. Grillo, S. D'Agostino, F. Della Sala, C. Giannini, D. Altamura, C. Oelsner, C. Kryschi, P. D. Cozzoli, *ACS Nano* **2013**, *7*, 7352.

[35] T. H. Larsen, M. Sigman, A. Ghezelbash, R. C. Doty, B. A. Korgel, *J. Am. Chem. Soc.* **2003**, *125*, 5638.

[36] Y.-B. Chen, L. Chen, L.-M. Wu, *Chem. Eur. J.* **2008**, *14*, 11069.

[37] P. Nørby, S. Johnsen, B. B. Iversen, *ACS Nano* **2014**, *8*, 4295.

[38] W. Han, L. Yi, N. Zhao, A. Tang, M. Gao, Z. Tang, *J. Am. Chem. Soc.* **2008**, *130*, 13152.

[39] W. Bryks, M. Wette, N. Velez, S. Hsu, A. R. Tao, *J. Am. Chem. Soc.* **2014**, *136*, 6175.

[40] L. Liu, C. Liu, W. Fu, L. Deng, H. Zhong, *ChemPhysChem* **2015**, DOI: 10.1002/cphc.201500627.

[41] L. Carbone, C. Nobile, M. De Giorgi, F. Della Sala, G. Morello, P. Pompa, M. Hytch, E. Snoeck, A. Fiore, I. R. Franchini, M. Nadasan, A. F. Silvestre, L. Chiodo, S. Kudera, R. Cingolani, R. Krahne, L. Manna, *Nano Lett.* **2007**, *7*, 2942.

[42] M. V. Kovalenko, M. Scheele, D. V. Talapin, *Science* **2009**, *324*, 1417.

[43] M. Zanella, L. Maserati, M. Pernia Leal, M. Prato, R. Lavieville, M. Povia, R. Krahne, L. Manna, *Chem. Mater.* **2013**, *25*, 1423.

[44] R. Pearson, *J. Am. Chem. Soc.* **1963**, *85*, 3533.

[45] C. Bullen, J. van Embden, J. Jasieniak, J. E. Cosgriff, R. J. Mulder, E. Rizzardo, M. Gu, C. L. Raston, *Chem. Mater.* **2010**, *22*, 4135.

[46] E. Dilena, Y. Xie, R. Brescia, M. Prato, L. Maserati, R. Krahne, A. Paolella, G. Bertoni, M. Povia, I. Moreels, L. Manna, *Chem. Mater.* **2013**, *25*, 3180.

[47] B. Koo, R. Patel, B. A. Korgel, *J. Am. Chem. Soc.* **2009**, *131*, 3134.

[48] P. L. Saldanha, R. Brescia, M. Prato, H. Li, M. Povia, L. Manna, V. Lesnyak, *Chem. Mater.* **2014**, *26*, 1442.

[49] Y. Wang, M. Zhukovskyi, P. Tongying, Y. Tian, M. Kuno, *J. Phys. Chem. Lett.* **2014**, *5*, 3608.

[50] D. Zhang, A. B. Wong, Y. Yu, S. Brittman, J. Sun, A. Fu, B. Beberwyck, A. P. Alivisatos, P. Yang, *J. Am. Chem. Soc.* **2014**, *136*, 17430.

[51] I. Kriegel, J. Rodríguez-Fernández, A. Wisnet, H. Zhang, C. Waurisch, A. Eychmüller, A. Dubavik, A. O. Govorov, J. Feldmann, *ACS Nano* **2013**, *7*, 4367.

[52] H. Li, R. Brescia, R. Krahne, G. Bertoni, M. J. P. Alcocer, C. D'Andrea, F. Scotognella, F. Tassone, M. Zanella, M. De Giorgi, L. Manna, *ACS Nano* **2012**, *6*, 1637.

[53] C. Bouet, D. Laufer, B. Mahler, B. Nadal, H. Heuclin, S. Pedetti, G. Patriarche, B. Dubertret, *Chem. Mater.* **2014**, *26*, 3002.

[54] K. Miszta, D. Dorfs, A. Genovese, M. R. Kim, L. Manna, *ACS Nano* **2011**, *5*, 7176.

[55] Z. Zhuang, Q. Peng, B. Zhang, Y. Li, *J. Am. Chem. Soc.* **2008**, *130*, 10482.

[56] S. Li, H. Wang, W. Xu, H. Si, X. Tao, S. Lou, Z. Du, L. S. Li, *J. Colloid Interface Sci.* **2009**, *330*, 483.

[57] Y. X. Zhao, H. C. Pan, Y. Lou, X. Qiu, J. Zhu, C. Burda, *J. Am. Chem. Soc.* **2009**, *131*, 4253.

[58] M. Page, O. Niitsoo, Y. Itzhaik, D. Cahen, G. Hodes, *Energy Environ. Sci.* **2009**, *2*, 220.

[59] Y. Wu, C. Wadia, W. Ma, B. Sadtler, A. Alivisatos, *Nano Lett.* **2008**, *8*, 2551.

[60] R. C. Neville, *Solar Energy Conversion: The Solar Cell*, Elsevier, Amsterdam, **1995**.

[61] Q. Guo, H. W. Hillhouse, R. Agrawal, *J. Am. Chem. Soc.* **2009**, *131*, 11672.

[62] Y. Cao, M. S. Denny, J. V. Caspar, W. E. Farneth, Q. Guo, A. S. Ionkin, L. K. Johnson, M. Lu, I. Malajovich, D. Radu, H. D. Rosenfeld, K. R. Choudhury, W. Wu, *J. Am. Chem. Soc.* **2012**, *134*, 15644.

[63] D. B. Mitzi, O. Gunawan, T. K. Todorov, K. Wang, S. Guha, *Sol. Energy Mater. Sol. Cells* **2011**, *95*, 1421.

[64] T. K. Todorov, K. B. Reuter, D. B. Mitzi, *Adv. Mater.* **2010**, *22*, E156.

[65] C. Steinhagen, M. G. Panthani, V. Akhavan, B. Goodfellow, B. Koo, B. A. Korgel, *J. Am. Chem. Soc.* **2009**, *131*, 12554.

[66] Q. Guo, S. Kim, M. Kar, W. Shafarman, R. W. Birkmire, E. A. Stach, R. Agrawal, H. W. Hillhouse, *Nano Lett.* **2008**, *8*, 2982.

[67] O. O. Otelaja, D. Ha, H. Zhang, R. D. Robinson, *ACS Appl. Mater. Interfaces* **2014**, *6*, 18911.

[68] P. Lukashev, W. R. L. Lambrecht, T. Kotani, M. van Schilfgaarde, *Phys. Rev. B* **2007**, *76*, 195202.

[69] D. Dorfs, T. Härtling, K. Miszta, N. C. Bigall, M. R. Kim, A. Genovese, A. Falqui, M. Povia, L. Manna, *J. Am. Chem. Soc.* **2011**, *133*, 11175.

[70] X. Wang, M. T. Swihart, *Chem. Mater.* **2015**, *27*, 1786.

[71] S. Hsu, W. Bryks, A. R. Tao, *Chem. Mater.* **2012**, *24*, 3765.

[72] S.-W. Hsu, K. On, A. R. Tao, *J. Am. Chem. Soc.* **2011**, *133*, 19072.

[73] Y. Liu, Y. Deng, Z. Sun, J. Wei, G. Zheng, A. M. Asiri, S. B. Khan, M. M. Rahman, D. Zhao, *Small* **2013**, *9*, 2702.

[74] B. J. Beberwyck, Y. Surendranath, A. P. Alivisatos, *J. Phys. Chem. C* **2013**, *117*, 19759.

[75] W. van der Stam, A. P. Gantapara, Q. A. Akkerman, G. Soligno, J. D. Meeldijk, R. van Roij, M. Dijkstra, C. de Mello Donega, *Nano Lett.* **2014**, *14*, 1032.

[76] J. M. Luther, H. Zheng, B. Sadtler, A. P. Alivisatos, *J. Am. Chem. Soc.* **2009**, *131*, 16851.

[77] B. Sadtler, D. O. Demchenko, H. Zheng, S. M. Hughes, M. G. Merkle, U. Dahmen, L.-W. Wang, A. P. Alivisatos, *J. Am. Chem. Soc.* **2009**, *131*, 5285.

[78] W. van der Stam, E. Bladt, F. T. Rabouw, S. Bals, C. D. M. Donega, *ACS Nano* **2015**, *9*, 11430.

[79] H. Li, M. Zanella, A. Genovese, M. Povia, A. Falqui, C. Giannini, L. Manna, *Nano Lett.* **2011**, *11*, 4964.

[80] L. De Trizio, R. Gaspari, G. Bertoni, I. Kriegel, L. Moretti, F. Scotognella, L. Maserati, Y. Zhang, G. C. Messina, M. Prato, S. Marras, A. Cavalli, L. Manna, *Chem. Mater.* **2015**, *27*, 1120.

[81] D. Ha, A. H. Caldwell, M. J. Ward, S. Honrao, K. Mathew, R. Hovden, M. K. A. Koker, D. A. Muller, R. G. Hennig, R. D. Robinson, *Nano Lett.* **2014**, *14*, 7090.

[82] W. van der Stam, A. C. Berends, F. T. Rabouw, T. Willhammar, X. Ke, J. D. Meeldijk, S. Bals, C. de Mello Donega, *Chem. Mater.* **2015**, *27*, 621.

[83] E. Groeneveld, L. Witteman, M. Lefferts, X. Ke, S. Bals, G. Van Tendeloo, C. de Mello Donega, *ACS Nano* **2013**, *7*, 7913.

[84] H. C. Yoon, J. H. Oh, M. Ko, H. Yoo, Y. R. Do, *ACS Appl. Mater. Interfaces* **2015**, *7*, 7342.

[85] N. Demir, I. Oner, C. Varlikli, C. Ozsoy, C. Zafer, *Thin Solid Films* **2015**, *589*, 153.

[86] S. H. Park, A. Hong, J.-H. Kim, H. Yang, K. Lee, H. S. Jang, *ACS Appl. Mater. Interfaces* **2015**, *7*, 6764.

[87] J.-Y. Chang, L.-F. Su, C.-H. Li, C.-C. Chang, J.-M. Lin, *Chem. Commun.* **2012**, *48*, 4848.

[88] Z. Pan, I. Mora-Sero, Q. Shen, H. Zhang, Y. Li, K. Zhao, J. Wang, X. Zhong, J. Bisquert, *J. Am. Chem. Soc.* **2014**, *136*, 9203.

[89] F. Meinardi, H. McDaniel, F. Carulli, A. Colombo, K. A. Velizhanin, N. S. Makarov, R. Simonutti, V. I. Klimov, S. Brovelli, *Nat. Nanotechnol.* **2015**, *10*, 878.

[90] K. E. Knowles, T. B. Kilburn, D. G. Alzate, S. McDowall, D. R. Gamelin, *Chem. Commun.* **2015**, *51*, 9129.

[91] C.-W. Chen, D.-Y. Wu, Y.-C. Chan, C. C. Lin, P.-H. Chung, M. Hsiao, R.-S. Liu, *J. Phys. Chem. C* **2015**, *119*, 2852.

[92] W. Guo, X. Sun, O. Jacobson, X. Yan, K. Min, A. Srivatsan, G. Niu, D. O. Kiesewetter, J. Chang, X. Chen, *ACS Nano* **2015**, *9*, 488.

[93] V. Singh, I. J. Castellanos Beltran, J. Casamada Ribot, P. Nagpal, *Nano Lett.* **2014**, *14*, 597.

[94] J. Chang, E. R. Waclawik, *CrystEngComm* **2013**, *15*, 5612.

[95] J. J. M. Binsma, L. J. Giling, J. Bloem, *J. Cryst. Growth* **1980**, *50*, 429.

[96] X. Lu, Z. Zhuang, Q. Peng, Y. Li, *CrystEngComm* **2011**, *13*, 4039.

[97] L. De Trizio, M. Prato, A. Genovese, A. Casu, M. Povia, R. Simonutti, M. J. P. Alcocer, C. D'Andrea, F. Tassone, L. Manna, *Chem. Mater.* **2012**, *24*, 2400.

[98] L. Li, A. Pandey, D. Werder, B. P. Khanal, J. M. Pietryga, V. I. Klimov, *J. Am. Chem. Soc.* **2011**, *133*, 1176.

[99] C. Xia, L. Cao, W. Liu, G. Su, R. Gao, H. Qu, L. Shi, G. He, *CrystEngComm* **2014**, *16*, 7469.

[100] H. Zhong, Z. Bai, B. Zou, *J. Phys. Chem. Lett.* **2012**, *3*, 3167.

[101] M. Kruszynska, H. Borchert, J. Parisi, J. Kolny-Olesiak, *J. Am. Chem. Soc.* **2010**, *132*, 15976.

[102] H. Zhong, Y. Zhou, M. Ye, Y. He, J. Ye, C. He, C. Yang, Y. Li, *Chem. Mater.* **2008**, *20*, 6434.

[103] J. Tang, S. Hinds, S. Kelley, E. Sargent, *Chem. Mater.* **2008**, *20*, 6906.

[104] N. Bao, X. Qiu, Y.-H. A. Wang, Z. Zhou, X. Lu, C. A. Grimes, A. Gupta, *Chem. Commun.* **2011**, *47*, 9441.

[105] O. Yarema, D. Bozyigit, I. Rousseau, L. Nowack, M. Yarema, W. Heiss, V. Wood, *Chem. Mater.* **2013**, *25*, 3753.

[106] J. Xu, C. Lee, Y. Tang, X. Chen, Z. Chen, *ACS Nano* **2010**, *4*, 1845.

[107] S. E. Wark, C.-H. Hsia, Z. Luo, D. H. Son, *J. Mater. Chem.* **2011**, *21*, 11618.

[108] M. E. Norako, M. J. Greaney, R. L. Brutchey, *J. Am. Chem. Soc.* **2012**, *134*, 23.

[109] J. Wang, P. Liu, C. C. Seaton, K. M. Ryan, *J. Am. Chem. Soc.* **2014**, *136*, 7954.

[110] X. Liu, X. Wang, M. T. Swihart, *Chem. Mater.* **2015**, *27*, 1342.

[111] X. Wang, X. Liu, D. Yin, Y. Ke, M. T. Swihart, *Chem. Mater.* **2015**, *27*, 3378.

[112] M. Kruszynska, J. Parisi, J. Kolny-Olesiak, *Z. Naturforsch. A* **2014**, *69*, 2.

[113] J. B. Rivest, P. K. Jain, *Chem. Soc. Rev.* **2013**, *42*, 89.

[114] S. Gupta, S. V. Kershaw, A. L. Rogach, *Adv. Mater.* **2013**, *25*, 6923.

[115] X. Huang, S. Li, Y. Huang, S. Wu, X. Zhou, S. Li, C. L. Gan, F. Boey, C. A. Mirkin, H. Zhang, *Nat. Commun.* **2011**, *2*, 292.

[116] L. De Trizio, H. Li, A. Casu, A. Genovese, A. Sathya, G. C. Messina, L. Manna, *J. Am. Chem. Soc.* **2014**, *136*, 16277.

[117] C. D. M. Donega, *Phys. Rev. B* **2010**, *81*, 165303.

[118] E. Groeneveld, C. D. M. Donega, *J. Phys. Chem. C* **2012**, *116*, 16240.

[119] E. Groeneveld, S. van Berkum, M. M. van Schooneveld, A. Gloter, J. D. Meeldijk, D. J. van den Heuvel, H. C. Gerritsen, C. de Mello Donega, *Nano Lett.* **2012**, *12*, 749.

[120] M. V. Yakushev, F. Luckert, C. Faugeras, A. V. Karotki, A. V. Mudryi, R. W. Martin, *Appl. Phys. Lett.* **2010**, *97*, 152110.

[121] H. Y. Ueng, H. L. Hwang, *J. Phys. Chem. Solids* **1989**, *50*, 1297.

[122] C. Guillén, J. Herrero, *Phys. Status Solidi A* **2006**, *203*, 2438.

[123] Y. Shi, Z. Jin, C. Li, H. An, J. Qiu, *Appl. Surf. Sci.* **2006**, *252*, 3737.

[124] S. B. Zhang, S. Wei, A. Zunger, *Phys. Rev. B* **1998**, *57*, 9642.

[125] B. Chen, H. Zhong, W. Zhang, Z. Tan, Y. Li, C. Yu, T. Zhai, Y. Bando, S. Yang, B. Zou, *Adv. Funct. Mater.* **2012**, *22*, 2081.

[126] J. Jaffe, A. Zunger, *Phys. Rev. B* **1983**, *28*, 5822.

[127] T. Debnath, S. Maiti, P. Maity, H. N. Ghosh, *J. Phys. Chem. Lett.* **2015**, *6*, 3458.

[128] J. J. M. Binsma, L. J. Giling, J. Bloem, *J. Lumin.* **1982**, *27*, 35.

[129] J. J. M. Binsma, L. J. Giling, J. Bloem, *J. Lumin.* **1982**, *27*, 55.

[130] T. Omata, K. Nose, K. Kurimoto, M. Kita, *J. Mater. Chem. C* **2014**, *2*, 6867.

[131] I. T. Kraatz, M. Booth, B. J. Whitaker, M. G. D. Nix, K. Critchley, *J. Phys. Chem. C* **2014**, *118*, 24102.

[132] K. E. Knowles, H. D. Nelson, T. B. Kilburn, D. R. Gamelin, *J. Am. Chem. Soc.* **2015**, *137*, 13138.

[133] A. Shabaev, M. J. Mehl, A. L. Efros, *Phys. Rev. B* **2015**, *92*, 035431.

[134] C. D. M. Donega, R. Koole, *J. Phys. Chem. C* **2009**, *113*, 6511.

[135] W. W. Yu, L. Qu, W. Guo, X. Peng, *Chem. Mater.* **2003**, *15*, 2854.

[136] E. Groeneveld, C. Delerue, G. Allan, Y.-M. Niquet, C. D. M. Donega, *J. Phys. Chem. C* **2012**, *116*, 23160.

[137] J. Jasieniak, L. Smith, J. Van Embden, P. Mulvaney, M. Califano, *J. Phys. Chem. C* **2009**, *113*, 19468.

[138] I. Moreels, K. Lambert, D. Smeets, D. De Muynck, T. Nollet, J. C. Martins, F. Vanhaecke, A. Vantomme, C. Delerue, G. Allan, Z. Hens, *ACS Nano* **2009**, *3*, 3023.

[139] I. Moreels, K. Lambert, D. De Muynck, F. Vanhaecke, D. Poelman, J. C. Martins, G. Allan, Z. Hens, *Chem. Mater.* **2007**, *19*, 6101.

[140] L. Qin, D. Li, Z. Zhang, K. Wang, H. Ding, R. Xie, W. Yang, *Nanoscale* **2012**, *4*, 6360.

[141] M. Booth, A. P. Brown, S. D. Evans, K. Critchley, *Chem. Mater.* **2012**, *24*, 2064.

[142] V. I. Klimov, *J. Phys. Chem. B* **2000**, *104*, 6112.

[143] P. Yu, M. C. Beard, R. J. Ellingson, S. Ferrere, C. Curtis, J. Drexler, F. Luiszer, A. J. Nozik, *J. Phys. Chem. B* **2005**, *109*, 7084.

[144] H. Zhong, S. Lo, T. Mirkovic, Y. Li, Y. Ding, Y. Li, G. D. Scholes, *ACS Nano* **2010**, *4*, 5253.

[145] T. Omata, K. Nose, S. Otsuka-Yao-Matsuo, *J. Appl. Phys.* **2009**, *105*, 073106.

[146] X. Liu, X. Wang, M. T. Swihart, *Chem. Mater.* **2015**, *27*, 1342.

[147] J. S. Niezgoda, M. A. Harrison, J. R. McBride, S. J. Rosenthal, *Chem. Mater.* **2012**, *24*, 3294.

[148] M. A. Green, K. Emery, Y. Hishikawa, W. Warta, E. D. Dunlop, *Prog. Photovoltaics* **2013**, *21*, 1.

[149] S. Draguta, H. McDaniel, V. I. Klimov, *Adv. Mater.* **2015**, *27*, 1701.

[150] D. H. Jara, S. J. Yoon, K. G. Stamplecoskie, P. V. Kamat, *Chem. Mater.* **2014**, *26*, 7221.

[151] H. McDaniel, N. Fuke, N. S. Makarov, J. M. Pietryga, V. I. Klimov, *Nat. Commun.* **2013**, *4*, 2887.

[152] Y. Zhao, C. Riemersma, F. Pietra, R. Koole, C. D. M. Donegá, A. Meijerink, *ACS Nano* **2012**, *6*, 9058.

[153] Z. Krumer, S. J. Pera, R. J. A. van Dijk-Moes, Y. Zhao, A. F. P. de Brouwer, E. Groeneveld, W. G. J. H. M. van Sark, R. E. I. Schropp, C. de Mello Donegá, *Sol. Energy Mater. Sol. Cells* **2013**, *111*, 57.

[154] M. G. Debije, P. P. C. Verbunt, *Adv. Energy Mater.* **2012**, *2*, 12.

[155] X. Hu, R. Kang, Y. Zhang, L. Deng, H. Zhong, B. Zou, L.-J. Shi, *Opt. Express* **2015**, *23*, A858.

[156] Y. Wang, R. Hu, G. Lin, I. Roy, K.-T. Yong, *ACS Appl. Mater. Interfaces* **2013**, *5*, 2786.

[157] G. Ma, *ACS Appl. Mater. Interfaces* **2013**, *5*, 2835.

[158] A. M. Smith, M. C. Mancini, S. Nie, *Nat. Nanotechnol.* **2009**, *4*, 710.

[159] R. Koole, M. M. Van Schooneveld, J. Hilhorst, K. Castermans, D. P. Cormode, G. J. Strijkers, C. D. M. Donega, D. Vanmaekelbergh, A. W. Griffioen, K. Nicolay, Z. A. Fayad, A. Meijerink, W. J. M. Mulder, *Bioconjugate Chem.* **2008**, *19*, 2471.

[160] T. Skajaa, Y. Zhao, D. J. van den Heuvel, H. C. Gerritsen, D. P. Cormode, R. Koole, M. M. van Schooneveld, J. A. Post, E. A. Fisher, Z. A. Fayad, C. de Mello Donega, A. Meijerink, W. J. M. Mulder, *Nano Lett.* **2010**, *10*, 5131.

[161] T. Pons, E. Pic, N. Lequeux, E. Cassette, L. Bezdetnaya, B. Dubertret, *ACS Nano* **2010**, *4*, 2531.

[162] K. Yu, P. Ng, J. Ouyang, M. B. Zaman, A. Abulrob, T. N. Baral, D. Fatehi, Z. J. Jakubek, D. Kingston, X. Wu, X. Liu, C. Hebert, D. M. Leek, D. M. Whitfield, *ACS Appl. Mater. Interfaces* **2013**, *5*, 2870.

[163] J. J. Scragg, P. J. Dale, L. M. Peter, G. Zoppi, I. Forbes, *Phys. Status Solidi B* **2008**, *245*, 1772.

[164] C. Persson, *J. Appl. Phys.* **2010**, *107*, 053710.

[165] H. Matsushita, T. Ichikawa, A. Katsui, *J. Mater. Sci.* **2005**, *40*, 2003.

[166] H. Zhou, W.-C. Hsu, H.-S. Duan, B. Bob, W. Yang, T.-B. Song, C.-J. Hsu, Y. Yang, *Energy Environ. Sci.* **2013**, *6*, 2822.

[167] H. Yang, L. A. Jauregui, G. Zhang, Y. P. Chen, Y. Wu, *Nano Lett.* **2012**, *12*, 540.

[168] A. Shavel, D. Cadavid, M. Ibáñez, A. Carrete, A. Cabot, *J. Am. Chem. Soc.* **2012**, *134*, 1438.

[169] T. Rath, W. Haas, A. Pein, R. Saf, E. Maier, B. Kunert, F. Hofer, R. Resel, G. Trimmel, *Sol. Energy Mater. Sol. Cells* **2012**, *101*, 87.

[170] X. Lu, Z. Zhuang, Q. Peng, Y. Li, *Chem. Commun.* **2011**, *47*, 3141.

[171] A. D. Collord, H. W. Hillhouse, *Chem. Mater.* **2015**, *27*, 1855.

[172] G. Larramona, S. Bourdais, A. Jacob, C. Choné, T. Muto, Y. Cuccaro, B. Delatouche, C. Moisan, D. Péré, G. Dennler, *J. Phys. Chem. Lett.* **2014**, *5*, 3763.

[173] K. Ramasamy, M. A. Malik, P. O'Brien, *Chem. Commun.* **2012**, *48*, 5703.

[174] Q. Guo, G. Ford, W. Yang, B. C. Walker, E. A. Stach, H. W. Hillhouse, R. Agrawal, *J. Am. Chem. Soc.* **2010**, *132*, 17384.

[175] S. Bag, O. Gunawan, T. Gokmen, Y. Zhu, T. K. Todorov, D. B. Mitzi, *Energy Environ. Sci.* **2012**, *5*, 7060.

[176] C. Jiang, W. Liu, D. V. Talapin, *Chem. Mater.* **2014**, *26*, 4038.

[177] Y. Zou, X. Su, J. Jiang, *J. Am. Chem. Soc.* **2013**, *135*, 18377.

[178] C. Coughlan, A. Singh, K. Ryan, *Chem. Mater.* **2013**, *25*, 653.

[179] A. Singh, C. Coughlan, F. Laffir, K. M. Ryan, *ACS Nano* **2012**, *6*, 6977.

[180] S. Singh, P. Liu, A. Singh, C. Coughlan, J. Wang, M. Lusi, K. M. Ryan, *Chem. Mater.* **2015**, *27*, 4742.

[181] M. Ibáñez, R. Zamani, W. Li, A. Shavel, J. Arbiol, J. R. Morante, A. Cabot, *Cryst. Growth Des.* **2012**, *12*, 1085.

[182] X. Yu, A. Shavel, X. An, Z. Luo, M. Ibáñez, A. Cabot, *J. Am. Chem. Soc.* **2014**, *136*, 9236.

[183] A. Singh, H. Geaney, F. Laffir, K. M. Ryan, *J. Am. Chem. Soc.* **2012**, *134*, 2910.

[184] C. Jiang, J. Lee, D. V. Talapin, *J. Am. Chem. Soc.* **2012**, *134*, 5010.

[185] J. M. R. Tan, Y. H. Lee, S. Pedireddy, T. Baikie, X. Y. Ling, L. H. Wong, *J. Am. Chem. Soc.* **2014**, *136*, 6684.

[186] A. Khare, A. W. Wills, L. M. Ammerman, D. J. Norris, E. S. Aydil, *Chem. Commun.* **2011**, *47*, 11721.

[187] A. Singh, S. Singh, S. Levcenko, T. Unold, F. Laffir, K. M. Ryan, *Angew. Chem. Int. Ed.* **2013**, *52*, 9120; *Angew. Chem.* **2013**, *125*, 9290.

[188] K. Tanaka, Y. Miyamoto, H. Uchiki, K. Nakazawa, H. Araki, *Phys. Status Solidi A* **2006**, *203*, 2891.

[189] V. Lesnyak, C. George, A. Genovese, M. Prato, A. Casu, S. Ayyappan, A. Scarpellini, L. Manna, *ACS Nano* **2014**, *8*, 8407.

[190] S. Niki, M. Contreras, I. Repins, M. Powalla, K. Kushiya, S. Ishizuka, K. Matsubara, *Prog. Photovoltaics* **2010**, *18*, 453.

[191] W. Wang, M. T. Winkler, O. Gunawan, T. Gokmen, T. K. Todorov, Y. Zhu, D. B. Mitzi, *Adv. Energy Mater.* **2014**, *4*, 1301465.

[192] G. M. Ford, Q. Guo, R. Agrawal, H. W. Hillhouse, *Chem. Mater.* **2011**, *23*, 2626.

[193] A. D. Collord, H. W. Hillhouse, *Sol. Energy Mater. Sol. Cells* **2015**, *141*, 383.